Biogeosciences, 21, 711–729, 2024
https://doi.org/10.5194/bg-21-711-2024
© Author(s) 2024. This work is distributed under
the Creative Commons Attribution 4.0 License.

Biogeosciences Open Access EGU

Characterization of the benthic biogeochemical dynamics after flood events in the Rhône River prodelta: a data–model approach

Eva Ferreira[1,★], Stanley Nmor[1,★], Eric Viollier[1], Bruno Lansard[1], Bruno Bombled[1], Edouard Regnier[1], Gaël Monvoisin[2], Christian Grenz[3], Pieter van Beek[4], and Christophe Rabouille[1]

[1]Laboratoire des Sciences du Climat et de l'Environnement, LSCE–IPSL, CEA–CNRS–UVSQ–Université Paris-Saclay, 91198, Gif-sur-Yvette, France
[2]Géosciences Paris-Saclay (GEOPS), CNRS and Université Paris-Saclay, 91405, Orsay, France
[3]Mediterranean Institute of Oceanography (MIO), Aix-Marseille Université, Université de Toulon, CNRS, IRD, MIO UM 110, 13288, Marseille, France
[4]Laboratoire d'Etudes en Géophysique et Océanographie Spatiales (LEGOS), CNES–CNRS–IRD–Université Toulouse III – Paul Sabatier, 31400, Toulouse, France
★These authors contributed equally to this work.

Correspondence: Eva Ferreira (eva.ferreira@lsce.ipsl.fr)

Received: 15 September 2023 – Discussion started: 28 September 2023
Revised: 8 December 2023 – Accepted: 18 December 2023 – Published: 8 February 2024

Abstract. At the land–sea interface, the benthic carbon cycle is strongly influenced by the export of terrigenous particulate material across the river–ocean continuum. Episodic flood events delivering massive sedimentary materials can occur, but their short-term impact on carbon cycling is poorly understood. In this paper, we use a coupled data–model approach to estimate the temporal variations in sediment–water fluxes, biogeochemical pathways and their reaction rates during these abrupt phenomena. We studied one episodic depositional event in the vicinity of the Rhône River mouth (NW Mediterranean Sea) during the fall–winter of 2021/22. The distributions of dissolved inorganic carbon (DIC), sulfate (SO_4^{2-}) and methane (CH_4) were measured in sediment porewaters collected every 2 weeks before and after the deposition of a 25 cm sediment layer during the main winter flood event. Significant changes in the distribution of DIC, SO_4^{2-} and CH_4 concentrations were observed in the sediment porewaters. The use of an early diagenetic model (FESDIA) to calculate biogeochemical reaction rates and fluxes revealed that this type of flood event can increase the total organic carbon mineralization rate in the sediment by 75 % a few days after deposition. In this period, sulfate reduction is the main process contributing to the increase in total mineralization relative to non-flood deposition. The model predicts a short-term decrease in the DIC flux out of the sediment from 100 to 55 mmol m^{-2} d^{-1} after the deposition of the new sediment layer with a longer-term increase by 4 %, therefore implying an initial internal storage of DIC in the newly deposited layer and a slow release over relaxation of the system. Furthermore, examination of the stoichiometric ratios of DIC and SO_4^{2-} as well as model output over this 5-month window shows a decoupling between the two modes of sulfate reduction following the deposition – organoclastic sulfate reduction (OSR) intensified in the newly deposited layer below the sediment surface, whereas anaerobic oxidation of methane (AOM) intensified at depth below the former buried surface. The bifurcation depth of sulfate reduction pathways, i.e., the sulfate–methane transition zone (SMTZ), is shifted deeper by 25 cm in the sediment column following the flood deposition. Our findings highlight the significance of short-term transient biogeochemical processes at the seafloor and provide new insights into the benthic carbon cycle in the coastal ocean.

1 Introduction

River-dominated ocean margins (RiOMar) are crucial areas linking land and open ocean. They play a key role in marine nutrient and carbon cycles (McKee et al., 2004; Cai,

2011; Bauer et al., 2013; Bianchi et al., 2018). These dynamic environments are known to have high riverine input and sedimentation rates (Aller, 1998). Furthermore, coastal sediments account for 85 % of long-term organic carbon burial in the ocean, with deltaic environments accounting for the majority (Burdige, 2005), but they are also powerful biogeochemical reactors (Aller et al., 1996; Rassmann et al., 2016). The large deposition of riverine (or terrigenous) particulate organic matter (POM) on the seafloor can result not only in the storage of organic carbon (OC) but also in strong benthic mineralization rates, dominated by sulfate reduction and methanogenesis (Mucci et al., 2000; Burdige and Komada, 2011). In deltaic sediments, which receive large amounts of POM, anaerobic respiration is one of the most important pathways for the remineralization of organic carbon (Canfield, 2004; Canfield and Thamdrup, 2009; Pastor et al., 2011a). As an example, the prominent anoxic pathway in the Rhône River prodelta is sulfate reduction, accounting for approximately 70 % of the total organic carbon mineralization rate in these sediments (Pastor et al., 2011a). This anoxic mineralization of organic carbon is supplemented by methanogenesis, which can account for up to 35 % of total organic matter degradation in sediment where a portion of reactive organic matter remains after complete sulfate exhaustion (Egger et al., 2016). The methane fluxes are controlled by the anaerobic oxidation of methane (AOM) in the subsurface sulfate–methane transition zone (STMZ; Boetius et al., 2000). Together, these processes modulate anoxic-based carbon cycling in coastal and deltaic sediments, therefore generating large quantities of dissolved inorganic carbon (DIC), and RiOMar systems are often considered CO_2 sources to the atmosphere (Cai, 2011; Bauer et al., 2013).

Flood events are especially significant along river-dominated margins and particularly for smaller river systems where sediment transport to the ocean preferentially occurs during extreme precipitation events (Bourrin et al., 2008; Lee et al., 2015). These materials can be subjected to secondary transport by waves and currents with a repeated cycle of resuspension and deposition (Ulses et al., 2008; Moriarty et al., 2017) as they discharge to the adjacent deltas and shelves. Furthermore, episodic events are also important in determining the locations and magnitude of hotspots of OC burial on the coastal margin. This is especially true during large storms that can greatly increase both river discharge and sediment load, resulting in increased sediment discharge to depositional zones along the shelf (Eglinton, 2008). During flood periods, large amounts of sediment and terrigenous OM are delivered to the adjacent delta and shelf. For example, the Eel River (northern California) is a major source-to-sink conduit for large sediment transport, delivering between 60 % and 80 % of discharged fine-grained sediment to the adjacent marine depocenter during large winter storms (Wheatcroft and Sommerfield, 2005). Similar large depositions of sediment over relatively short periods of time have been documented elsewhere, near the island of Taiwan (Liu et al., 2013), in the Mekong Delta (Manh et al., 2014) or in the Yangtze River estuary depositional system (Dai et al., 2018) to name a few.

In the Rhône River (NW Mediterranean Sea), flood events can account for 80 % of annual terrigenous particle inputs (Antonelli et al., 2008; Eyrolle et al., 2012), which at times can deliver up to 30 cm of sediment deposition on the Rhône River prodelta located in the Gulf of Lion (Charmasson et al., 1998; Antonelli et al., 2008; Lansard et al., 2009; Cathalot et al., 2010). These sediments are mostly deposited in the prodelta, as previously shown by Wu et al. (2018) using beryllium-7 (^{7}Be), a natural short-life radionuclide which traces deposits of riverine suspended particulate matter (SPM). These winter events are abrupt and therefore difficult to document precisely. Consequently, few studies have been conducted on the biogeochemical response of coastal sediment following intense export of sediment and organic carbon (Cathalot et al., 2010; Pastor et al., 2018). Furthermore, we can expect that the frequency and intensity of flood events will increase as a result of climate change (Day et al., 2019; Lionello et al., 2023). However, due to the unpredictable nature of meteorological and flood events, it is difficult to monitor these intense events.

Many efforts have been made to incorporate biogeochemical processes operating in the sediment into mathematical models (Berner, 1980). These early diagenetic models have been heavily used to investigate the fate and transport of a selected set of chemical species on the seafloor (Aguilera et al., 2005). Recent non-steady-state diagenetic models based on previous numerical representations of sediment transport and reactions (Rabouille and Gaillard, 1991; Soetaert et al., 1996; Wang and Van Cappellen, 1996; Berg, 2003) have demonstrated the importance of explicitly depicting event-driven processes (De Borger et al., 2021; Nmor et al., 2022). The benefit of these models is that they take deposition thickness into consideration as a vital parameter for reproducing such an episodic event (Nmor et al., 2022). Combining sediment and porewater data can help to constrain model inputs and aid in the simulation of such depositional events.

The goal of this study was to examine the transient evolution of benthic carbon mineralization processes and their impact on sediment–water exchange during a flood event marked by large sediment deposition. We intend to characterize and quantify the changes that occur in several biogeochemical pathways and fluxes during these periods of substantial deposition of sedimentary material. We used a dualistic approach to solve this question by combining bi-monthly observational data on sediment evolution with a non-steady-state early diagenetic model that calculates biogeochemical rates and fluxes. This multivariate perspective gave us a better understanding of the factors that control organic carbon remineralization and the relative shares of organoclastic sulfate reduction (OSR) and methanogenesis, together with anaerobic oxidation of methane (AOM). We therefore addressed the question of how massive material deposition affects the biogeochemical carbon cycle in coastal sediment.

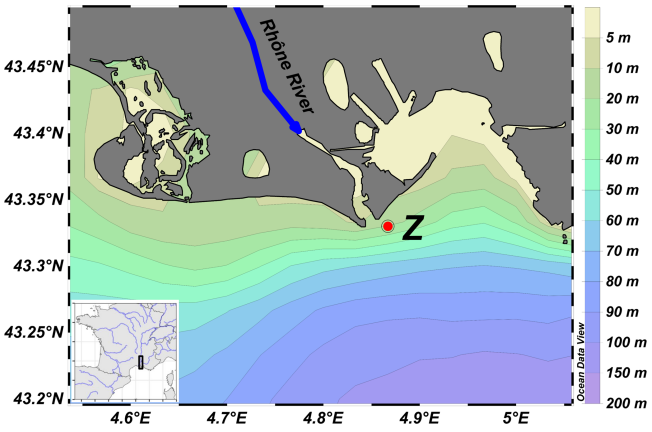

Figure 1. Map of the Gulf of Lion (Rhône prodelta) including the location of the sampling station (station Z/Mesurho).

2 Materials and methods

2.1 Study site

The Rhône River is the main source of freshwater, nutrients, organic matter and sediment for the Mediterranean Sea (Durrieu de Madron et al., 2000). It is characterized by a drainage basin of 97 800 km^2 and an average water discharge of 1700 m^3 s^{-1} with a marked seasonality between low-water discharge (< 700 m^3 s^{-1}) in summer and high-water discharge (> 3000 m^3 s^{-1}) in fall and winter (Pont et al., 2002). The Rhône River turbidity plume extends mainly southwestward into the Gulf of Lion, with an average thickness of 1 m (up to 5 m) (Many et al., 2018). The Gulf of Lion is a microtidal, wave-dominated system, with a tidal range of 30 to 50 cm. Due to salt-induced flocculation (Thill et al., 2001), most suspended particulate matter (SPM) carried out by the Rhône River settles in front of the mouth, on the prodelta (Maillet et al., 2006; Estournel et al., 2023). The study site (station Z/Mesurho, water depth 20 m, Fig. 1) is located on the delta front, at a distance of 2 km from the river mouth, and is characterized by a mean apparent accumulation rate of up to 35 to 48 cm yr^{-1} (Charmasson et al., 1998). The site is defined by geographic coordinates (see Table 1), but the constraints of sea work (e.g., ship drift) lead to a positioning variability estimated at a perimeter of 60 m around these coordinates.

The fall–winter monitoring (AMOR SB) took place bimonthly from November 2021 to March 2022 (Table 1) when the weather permitted with sampling cruises on board the RV *Antédon II* (IFREMER FOF). The Rhône River flows were recovered from the HydroPortail database at the Tarascon–Beaucaire station (hydrometric station V720001002). The SPM content was recovered from the database of the Rhône Sediment Observatory. Missing data are estimated empirically using the relationship between flows and Cesium (Cs) determined from sediment rating curves (Lepage et al., 2022).

Table 1. Temporal sampling coverage and location of sampling sites during the winter season of 2021/22.

Cruises	Date	Rhône River water flow (m^3 s^{-1})	Lat (° N)	Long (° E)
SB7	3 Nov 2021	2057	43°19.066′	4°52.023′
SB7bis	19 Nov 2021	830	43°19.066′	4°52.023′
SB8	1 Dec 2021	905	43°19.032′	4°51.952′
SB9	7 Jan 2022	2533	43°19.111′	4°52.048′
SB9bis	19 Jan 2022	1318	43°19.096′	4°52.034′
SB10bis	23 Feb 2022	1972	43°19.131′	4°52.071′
SB11	8 Mar 2022	1110	43°19.108′	4°52.089′

2.2 Sediment and porewater sampling and analyses

Sediment cores were collected at each of the cruises reported in Table 1 with a UWITEC single corer (USC 09000) equipped with a weight of 30 kg. The length of the coring tubes was 120 cm with an internal diameter of 9 cm. At least two sediment cores were retrieved with a well-preserved sediment–water interface (SWI). One core was dedicated to the sampling of sediment porewaters, and the second core was cut into slices for further laboratory analysis. Sediment porewaters were extracted using syringes connected to porous Rhizon with an average pore diameter of 0.1 µm (Seeberg-Elverfeldt et al., 2005). The vertical sampling resolution was 2 cm for the first 10 cm and then 4 cm down to the end of the core. At each sampled depth, between 12 and 15 mL of porewater was extracted. The content of each syringe was immediately subsampled after extraction. For dissolved inorganic carbon (DIC) analysis, 5 mL samples were poisoned with 10 µL of supersaturated $HgCl_2$ and stored in 10 mL glass vials at 4 °C until analysis. Concentrations of DIC were analyzed by a LI-COR infrared detector with a DIC analyzer AS-C1 (Apollo SciTech) on 0.75 mL samples, as described in Rassmann et al. (2016). The relative uncertainty was ± 0.2 %. For SO_4^{2-} analysis, 2 mL was subsampled and acidified with 8 µL of HNO_3 and stored in Eppendorf tubes at 4 °C until analysis. Concentrations of SO_4^{2-} were analyzed on 100 µL samples with a liquid-phase ion chromatography system (ICS-1000 Dionex™) with AG14 precolumn, AS14 column and AERS 500 suppressor configuration at the Géosciences Paris-Saclay laboratory, as described in Rassmann et al. (2020). The relative uncertainty was ± 0.3 %.

On the same core, sub-core samples were taken for CH_4 analysis with a 5 cm resolution in side holes using two sharpened 5 mL syringes of 1 cm diameter. The contents of two syringes of the same level were quickly introduced into empty pre-weighed 60 mL vials with 35 mL of potassium hydroxide (KOH, 1 mol L^{-1}) (Magen et al., 2014). The vials were then directly sealed, shaken and stored upside

down in the dark. Back in the laboratory, CH_4 concentrations were analyzed with a micro-gas chromatograph Agilent Technologies® 490 GC. Measurements were made in three 60 s analyses, with 1.5 mL gas samples taken from the "headspace" (Rassmann et al., 2020). The calibration was performed with a standard gas of CH_4 at 104 ppm with a reproducibility of 1 %. Data obtained indicate a percentage of CH_4 in the headspace which allows the calculation of CH_4 quantity in headspace by dividing the volume of CH_4 by the molar volume of a gas at 1 atm. This quantity is then used to back-calculate the CH_4 concentration in the porewater using porosity and sediment weight, with an estimated accuracy of 5 %.

The second sediment core was sliced as follows: every 0.5 cm for the first 2 cm of the core, every 1 cm down to 10 cm, every 2 cm down to 20 cm and finally every 5 cm for the rest of the core. Sediment samples were stored in freezer bags preserved at −20 °C. One part of the sediment samples was used to determine the organic carbon (OC) content, reported in percent dry weight sediment. Sediment layers were freeze-dried, crushed and decarbonated by successive acidification baths (HCl 10 %) over several days after rinsing. Homogenized and accurately weighed subsamples were analyzed by a Carlo Erba NA 1500 Elemental Analyzer. The average OC contents were calculated for the first 30 cm sediment before and after the flood.

Another part of this sediment core was used to analyze beryllium-7 (^{7}Be) activity within 3 months of sample collection using low-background gamma-ray spectrometry at the LAFARA underground laboratory (van Beek et al., 2013). Between 8.0 and 12.5 g of dry sediment was analyzed during 48 h using a Mirion Canberra planar detector (germanium crystal of 230 cm^3) equipped with Lynx (Mirion Canberra) electronics and an electric cooling system (CryoPulse® 5 plus provided by Mirion Canberra). The ^{7}Be activities are reported with 2σ uncertainties.

2.3 Stoichiometric ratio

The anaerobic mineralization of buried organic matter by sulfate reduction (Reaction R1) and the anaerobic methane oxidation (AOM; Reaction R2) reactions provide theoretical stoichiometric ratios ($r_{c:s}$) of SO_4^{2-} consumption to bicarbonate ion production.

$$2CH_2O + SO_4^{2-} \rightarrow 2HCO_3^- + H_2 \quad \text{(R1)}$$

$$CH_4 + SO_4^{2-} \rightarrow HCO_3^- + HS^- + H_2O \quad \text{(R2)}$$

This ratio can be used to identify the key process that dominates mineralization in sediments from porewater measurements (Burdige and Komada 2011). The $r_{c:s}$ values (Eq. 1) of the present dataset were calculated as described by Burdige and Komada (2011). The slope of the property–property plot of ΔDIC versus ΔSO_4^{2-} was corrected by the diffusion coefficient ratio at in situ temperature (Li and Gregory 1974) in order to eliminate the effect of transport by diffusion (Burdige and Komada, 2011).

$$r_{c:s} = \frac{D_{HCO_3^-}}{D_{SO_4^{2-}}} \cdot \frac{\Delta DIC}{\Delta SO_4^{2-}} \quad (1)$$

Before the flood event $r_{c:s}$ values were calculated on the whole core. After the deposition event, two $r_{c:s}$ values were calculated as a function of depth, the first on a surface layer between 1 and 25 cm and the second from 25 cm to the bottom of the core.

2.4 Numerical modeling

The model FESDIA is a time-dependent early diagenesis model designed for perturbation studies. This model is made up of a set of coupled non-linear partial differential equations that describe the distribution of porewater species at different depths. This model is notable for its ability to simulate event-driven dynamics such as sudden sediment deposition as a result of flood input. Details of the model formulations and equations were described in Nmor et al. (2022). Here, we briefly outline important processes involving sulfur and methane cycle as well as the parameterization considered necessary for the representation of the winter flood situation the Rhône River prodelta.

The model considers the entire sequence of OM remineralization pathways in the sediment, including OM remineralization coupled to oxygen; nitrogen; iron and manganese oxides; sulfate; and, finally, methane production. In general, organic matter oxidation follows the formalism of a cascading sequence of these terminal electron acceptors (Canfield and Thamdrup, 2009). The organic matter modeled is made up of two degradable fractions with different reactivities. This decay is modeled as a first-order rate law, and the contribution of the different mineralization pathways to total OC mineralization is determined by the limitation and inhibition of the different primary oxidants in the sediment. Secondary reactions involving reduced species include nitrification, reoxidation of reduced metals, methane oxidation (see below) via oxygen, sulfide reoxidation by iron and manganese hydr(oxides), and iron-sulfide precipitation. Table 2 contains a summary of the parameters used in the model. Either these values were derived from previous steady-state modeling works in the Rhône prodelta sediment (Pastor et al., 2011a; Ait Ballagh et al., 2021), or in other cases, where no model parameter value was known for the Rhône prodelta sediment, values from other literature sources were calibrated with the observed data.

2.5 Methanogenesis

Below the sulfidic zone, organic carbon is remineralized via methanogenesis. The product of this fermentation of organic matter in depth by anaerobic archaea is methane (CH_4) and

Table 2. Summary of parameters used in the FESDIA model. Types are as follows: (I) independent parameters derived from experiments or field observation external to actual data being simulated, (C) constrained parameters obtained from a range of literature sources, and (M) model-derived parameters fitted to the observed data. FDET refers to labile fraction and SDET refers to semi-labile fraction of organic carbon. Literature sources include (1) Pastor et al. (2011a), (2) Soetaert et al. (1996), (3) Ait Ballagh et al. (2021), (4) Rassmann et al. (2020), (5) Wang and Van Cappellen (1996), and (6) Van Cappellen and Gaillard (2018).

Parameter	Description	Value	Unit	Type	Source
Cflux	total organic C deposition	15 000	$\mathrm{nmol\,C\,cm^{-2}\,d^{-1}}$	I	1
pFast	part FDET in carbon flux	0.5	–	C	1
FeOOHflux	deposition rate of FeOOH	7000	$\mathrm{nmol\,C\,cm^{-2}\,d^{-1}}$	M	–
MnO_2flux	flux of Mn oxides	1500	$\mathrm{nmol\,C\,cm^{-2}\,d^{-1}}$	M/C	–/5
NCrFdet	NC ratio FDET	0.14	$\mathrm{mol\,N\,mol\,C^{-1}}$	I	2
NCrSdet	NC ratio SDET	0.1	$\mathrm{mol\,N\,mol\,C^{-1}}$	I	2
O_{2bw}	upper boundary O_2	238	$\mathrm{mmol\,m^{-3}}$	M	–
NO_{3bw}	upper boundary NO_3	0	$\mathrm{mmol\,m^{-3}}$	M	–
NH_{3bw}	upper boundary NH_3	0	$\mathrm{mmol\,m^{-3}}$	M	–
CH_{4bw}	upper boundary CH_4	0	$\mathrm{mmol\,m^{-3}}$	M	–
DIC_{bw}	upper boundary DIC	2360	$\mathrm{mmol\,m^{-3}}$	M	–
Fe_{bw}	upper boundary Fe^{2+}	0	$\mathrm{mmol\,m^{-3}}$	M	–
H_2S_{bw}	upper boundary H_2S	0	$\mathrm{mmol\,m^{-3}}$	M	–
SO_{4bw}	upper boundary SO_4^{2-}	33 246	$\mathrm{mmol\,m^{-3}}$	M	–
Mn_{bw}	upper boundary Mn^{2+}	0	$\mathrm{mmol\,m^{-3}}$	M	–
w	advection rate	0.08	$\mathrm{cm\,d^{-1}}$	M	–
por0	surface porosity	0.83	–	I	4
pordeep	deep porosity	0.65	–	I	1/4
porcoeff	porosity decay coefficient	2	cm	I	1/4
biot	bioturbation coefficient	0.05	$\mathrm{cm^2\,d^{-1}}$	C	1
biotdepth	depth of sediment mixed layer	5	cm	I	3
biotatt	attenuation coeff below biotdepth	1	cm	I	3
irr	bio-irrigation rate constant	0.3	$\mathrm{d^{-1}}$	M	–
irrdepth	depth of irrigated layer	7	cm	I	3
irratt	attenuation coeff below irrdepth	1	cm	I	3
temperature	temperature	15.6	dg C	M	–
salinity	salinity	37.8	psu	M	–
TOC0	refractory carbon conc.	1.0	%	M	–
rFast	decay rate FDET	0.5	$\mathrm{d^{-1}}$	C	1
rSlow	decay rate SDET	0.0031	$\mathrm{d^{-1}}$	C	1
rH_2SMnO_x	rate of reoxidation of H_2S by MnO_x	0.001728	$\mathrm{cm^3\,nmol^{-1}\,d^{-1}}$	M/C	–/5
rFeS	rate constant of FeS production	0.5	$\mathrm{cm^3\,nmol^{-1}\,d^{-1}}$	I	5
rMnFe	rate constant of Fe reoxidation with MnOx	6.48×10^{-6}	$\mathrm{cm^3\,nmol^{-1}\,d^{-1}}$	M/C	–/5
rAOM	rate constant for AOM	3×10^{-5}	$\mathrm{cm^3\,nmol^{-1}\,d^{-1}}$	C	6
alphaFDET	Enrichment factor for FDET	4	–	M	–
alphaSDET	Enrichment factor for SDET	1.8	–	M	–
$alphaFeOOH_A$	Enrichm. factor for $FeOOH_A$	1	–	M	–
$alphaFeOOH_B$	Enrichm. factor for $FeOOH_B$	1	–	M	–
$alphaMnO_{2A}$	Enrichm. factor for MnO_{2A}	1	–	M	–
$alphaMnO_{2B}$	Enrichm. factor for MnO_{2B}	1	–	M	–

can be represented as follows (Reaction 3):

$$2CH_2O \rightarrow CH_4 + CO_2. \quad (2)$$

In the Rhône River proximal prodelta, high sedimentation deposition ($> 30\,\mathrm{cm\,yr^{-1}}$) and high particulate organic carbon flux ($657\,\mathrm{g\,C\,m^{-2}\,yr^{-1}}$) have been observed (Durrieu de Madron et al., 2000; Pastor et al., 2011a). As a result, high methane production at depth is likely (Garcia-Garcia et al., 2006; Pozzato et al., 2018; Rassmann et al., 2020). In the model, the accumulation of methane derived from carbon remineralization is limited by the equilibrium between dissolved and free gas, which can occur at around 90 ppm (or 6 mM) in shallow sediment of the Rhône prodelta (Garcia-Garcia et al., 2006). This is done by considering methane

removal into free gas as follows (Eq. 2):

$$CH_{4gas} = \max(0, k_{gas} \cdot (CH_4 - CH_{4equil})), \quad \text{(R3)}$$

where CH_{4equil} is the equilibrium concentration for which observed and simulated methane goes into hydrate or gas phases.

2.6 Methane oxidation

The methane produced deep down in the sediment can diffuse upward and be reoxidized in the presence of oxygen (Reaction 4) with a simple first-order rate expression used in the model:

$$CH_4 + 2O_2 \rightarrow CO_2 + 2H_2O. \quad \text{(R3)}$$

However, an important part of this investigation involves the interaction between the sulfur and methane cycle. Critical to this link is the role of anaerobic oxidation of methane (AOM) (Reaction 2). The AOM is a vital microbial process which acts as a barrier to the extent of the upward methane flux from the deeper sediment. The AOM occurs at the nexus of sulfate depletion and methane production, at a depth horizon typically referred to as the sulfate–methane transition zone (SMTZ). This reaction is modeled as a first-order process involving both CH_4 and SO_4^{2-}.

$$AOM = rAOM \times CH_4 \times SO_4^{2-}, \quad (4)$$

where rAOM is the constant apparent AOM reaction rate. As this pathway of sulfate reduction occurs at a much slower rate than the sulfate reduction coupled to organic carbon oxidation (Van Cappellen and Gaillard, 2018), the value R_{AOM} was set to $3 \times 10^{-5}\,cm^3\,nmol^{-1}\,d^{-1}$.

2.7 Model configuration

The FESDIA model was implemented in a 1 m sediment domain with variable depth resolution. Sediment thickness increases from 1 mm at the surface to about 6 cm at the base of the domain. For our application, we used a sedimentation rate of $30\,cm\,yr^{-1}$ (Lansard et al., 2009) and the degradation constant of the labile carbon (rFast) was tuned to $0.5\,d^{-1}$. Other parameters relevant to this particular simulation were derived from other literature sources, and a list is provided in Table 2.

Porosity was modeled as an exponential decay with depth increasing from 0.83 at the surface to an asymptotic value of 0.65 at depth according to observations. Bioturbation was constant in the first 5 cm with a rate of $0.05\,cm^2\,d^{-1}$ and exponentially attenuated below with reduced fauna activity. Based on the low bioturbation rate observed at station Z and the dominance of flood deposition in sedimentation (Pastor et al., 2011a), the FESDIA model is used with a constant bioturbation rate over the study period (Nmor et al., 2022). Solute pumping via bio-irrigation was also modeled. A summary of the parameters used in the model is given in Table 2.

The deposition of flood materials was carried out in a similar manner to that described in Nmor et al. (2022). Here, we imposed a singular flood scenario with a thickness of 25 cm. The inclusion of this single event was dictated by the dominant presence of an abnormally high SPM concentration observed during the winter flooding season as recorded by the SORA monitoring station located in Arles, 40 km upstream of the river mouth (Fig. 2). As such, we assumed that deposition during this flood period only lagged by a few days the observance of a high SPM load. This forces the date used for the deposition in the model (3 January 2022). The deposited material thickness in the model is indirectly diagnosed using measurement of porewater solute distribution and strengthened by beryllium-7 data collected after particle settling (see Sect. 3). During the time of the event, the model assumes that the solute concentration within the perturbed layer is homogenous and that it resets to the bottom-water concentration.

As described in Nmor et al. (2022), the deposited flood layer can have a different particulate composition than the pre-existing sediment. Depending on the nature of the flood, it can be enriched or depleted in reactive compounds for the two pools of organic matter (C_{fast}^{org}, C_{org}^{slow}), of manganese oxides (MnO_{2A} and MnO_{2B}) and of amorphous iron ($FeOH_A$ and $FeOOH_B$). This is translated in the model by the enrichment factor (α), specific to each type of compound, and was set to the values reported in Table 2.

3 Results

3.1 Water discharge and SPM concentrations in the Rhône River

During the sampling period (November 2021–March 2022), the discharge rate of the Rhône River varied significantly with monthly fluctuations (Fig. 2). The average river discharge during this period was about $1800\,m^3\,s^{-1}$. Daily discharges ranged from $553\,m^3\,s^{-1}$, during the low-flow period, to $5045\,m^3\,s^{-1}$, in January 2023. This maximum river discharge is 3 times larger than the mean discharge experienced during this period and 2 times larger than the other monthly peaks observed in November, December and February. This highest discharge coincides with the maximum of SPM which is as high as $1420\,mg\,L^{-1}$. This high load of SPM is clearly discernible compared to the average SPM of $64\,mg\,L^{-1}$ experienced within the 5-month duration of the sampling campaign. The other peak in SPM recorded in November 2022 was also relatively small ($91\,mg\,L^{-1}$).

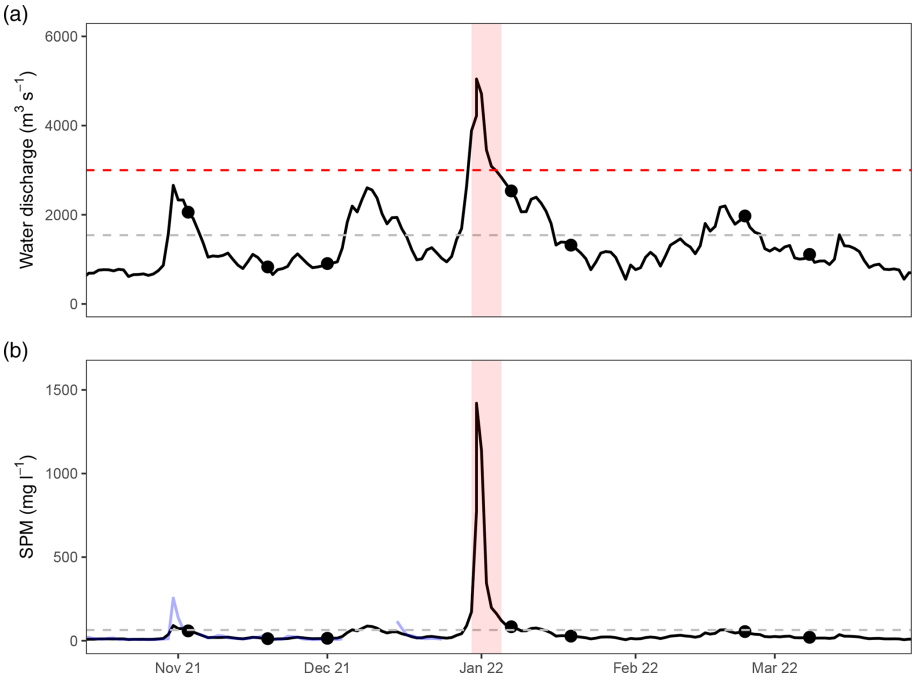

Figure 2. (a) Mean daily water discharge of the Rhône River at Beaucaire–Tarascon, located 60 km upstream of the river mouth. The dashed grey line symbolizes the average water discharge level. The dashed red line symbolizes the flood level at Beaucaire–Tarascon with the flood period symbolized with the red bar. **(b)** Total suspended particulate matter (SPM) concentration in the Rhône River at SORA station in Arles. The dashed grey line symbolizes the average sediment concentration. The seven cruises are indicated by the black dots.

3.2 Porewater composition of DIC, SO_4^{2-} and CH_4 and its comparison to model outputs

The depth profiles of measured and simulated concentrations of DIC, SO_4^{2-} and CH_4 are presented in Fig. 3 for all time points during the winter monitoring. Prior to the flood deposition, porewater sulfate concentrations were constant in the first 10 cm of the sediment with concentrations of 31–32 mM. Below, SO_4^{2-} concentrations decrease smoothly with depth to 40 cm, where no or little sulfate was detected. The model reproduced a strong gradient of decreasing sulfate concentrations between 10 and 40 cm. This gradient associated with sulfate reduction resulted in a vertically integrated sulfate consumption rate obtained by the model of 97 mmol C m^{-2} d^{-1} prior to the deposition event. In contrast, methane was virtually zero in the upper 20 cm of the sediment. From 25 cm downward, methane built up in the porewaters, with CH_4 rising up to 5–6 mM with depth. The trend in the data, supported by the model, indicated that a CH_4 gradient exists at depth. At depth, the entire contribution of methanogenesis to organic carbon mineralization as calculated by the model was 9 mmol C m^{-2} d^{-1}.

The net product of mineralization pathways is DIC. The measured DIC concentration in the bottom waters was 2.36 mM but gradually increased with depth up to 40 mM at the bottom of the sediment core. This DIC maximum at 40 cm was well reproduced by the model simulations due to the accumulation of organic matter mineralization. In general, DIC and SO_4^{2-} profiles were symmetrical (negatively correlated) throughout the time series. Before the major flood deposition, the changes in DIC, SO_4^{2-} and CH_4 profiles were limited. However, slight heterogeneity in the porewater profile (three different sampling times) led to slightly less remarkable agreement between both model and data. Nonetheless, significant degrees of correspondence between the model and data were generally observed with a correlation coefficient higher than 0.8.

After the flood deposition at the end of December 2021, all concentration profiles of chemical species in the sediment porewaters showed significant changes. The flood input resulted in the intrusion of sulfate-rich porewater (> 25 mM) down to 25 cm together with relatively low DIC concentration (< 10mM). This nearly constant sulfate concentration in the data was clearly reproduced by the model. Below this depth, the profile was similar to the pre-flood situation with a slightly less steep gradient. The strong sulfate consumption between 40 and 75 cm was observed in the data and simulated by the model. For all three species (DIC, SO_4^{2-} and CH_4), the correlation between observed data and model was significant ($r > 0.8$). In both cases, a consistent increase to 6 mM for CH_4 and to 50 mM for DIC occurred, while SO_4^{2-} reached zero at 60 cm. The depth of appearance of CH_4 was also shifted from an average position of 30 cm before the flood to a depth of 60 cm after the flood deposition. The max-

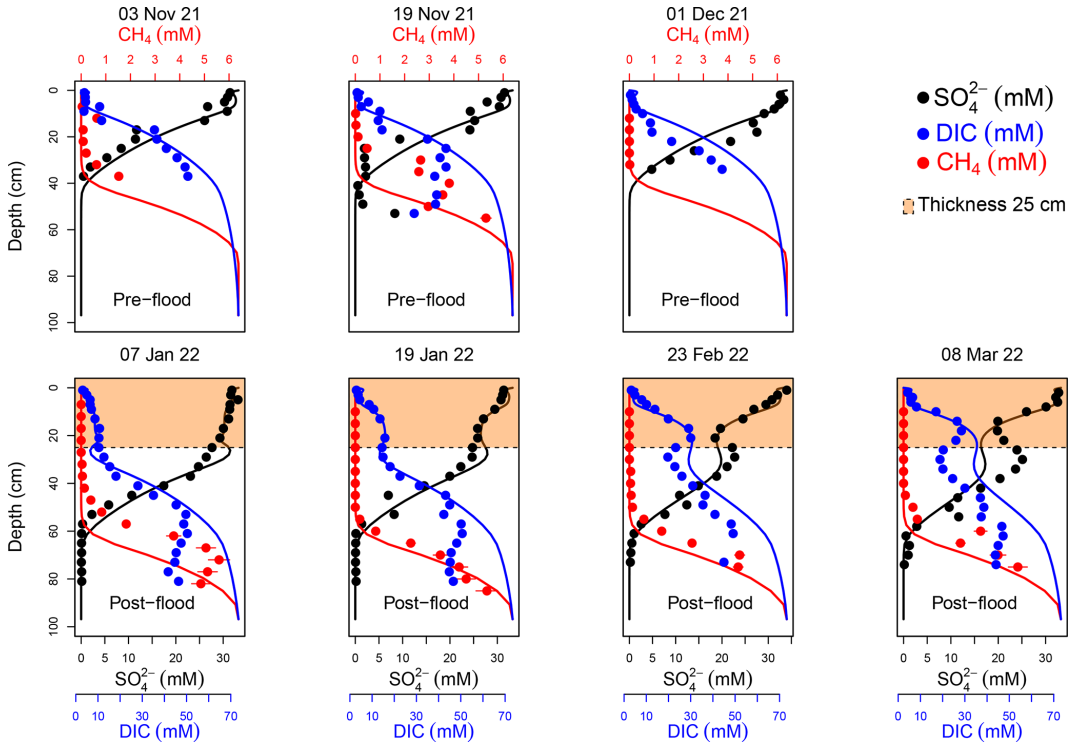

Figure 3. Vertical distribution of dissolved inorganic carbon (DIC), sulfate (SO_4^{2-}) and methane (CH_4) concentrations in sediment porewaters. Dots represent the measured porewater data, and lines denote the model result. The orange zone shows the deposited flood layer.

imum in both CH_4 and DIC concentrations occurred at 70 and 60 cm, respectively. In addition, the model reproduced the sulfate–methane transition zone observed in the data. The model was able to obtain a satisfactory fit generally over the 60 cm depth. Below this depth, the simulated profiles obtained in January 2022 showed a slight deviation from the measured profiles. Below the flood layer, the sediment profiles barely changed in the first month after the deposition of the flood layer. An excellent agreement between the model and data is observed. Over the longer term, little change in the SMTZ was observed over the 2 months following flood deposition. The upward diffusion of CH_4 was virtually not discernible in the CH_4 profiles. At 2 months after the event, the slow upward shift in CH_4 was still undetectable and the depth of appearance of CH_4 was still around 60 cm.

In the upper layer, all solutes were slowly and steadily reorganized 1 month after deposition. Sulfate was still present down to 60 cm, with a significant decrease in the top 20 cm, and DIC accumulation in this layer of the sediment was obvious in both data and model results. However, the gradual establishment of a new gradient in this layer begins after that. As of February 2022, two gradients can be seen, one between 19 and 29 cm and the other between 40 and 61 cm.

3.3 Beryllium-7 (^{7}Be)

The vertical distribution of beryllium-7 measured after the flood showed significant activity down to 30 cm (Fig. 4). Because of the relatively short half-life of ^{7}Be ($t_{1/2} = 53.3$ d), the presence of ^{7}Be within this active upper zone suggests a recently deposited layer. Higher ^{7}Be activities (up to 58.9 Bq kg^{-1}) are observed in the upper 1.5 cm. Overall, the ^{7}Be activities range between 19 and 54 Bq kg^{-1} at this depth interval and can be considered relatively homogenous, considering error bars (2σ). No significant ^{7}Be activity is observed below 30 cm. The significant ^{7}Be activities determined as deep as 30 cm thus likely indicate a recent, instantaneous deposition event. This depth interval likely reflects the thickness of the layer deposited following the flood event.

3.4 Organic carbon content

The average organic carbon content (OC) of sediment cores collected before and after the main flood event is shown Table 3. The pre-flood sediment had an average OC of 1.3 ± 0.3 % dw; for the same period the model simulated an average OC of 1.1 % dw. The shape of the pre-flood OC profile showed a decrease with depth, starting at 1.8 ± 0.2 % dw at the SWI and declining to 0.9 ± 0.2 % dw at 22 cm.

In contrast, post-flood OC distribution exhibited a less clear pattern in its variation with depth with overall larger

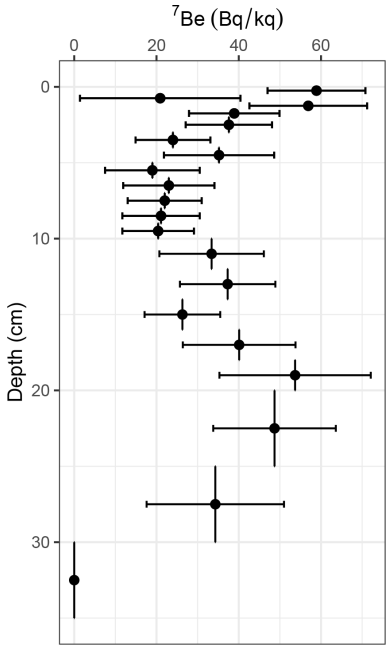

Figure 4. Vertical distribution of beryllium-7 activities in the sediment core collected after the flood event (7 January 2022); vertical bars represent the thickness of the sediment layer on which analysis was conducted.

Table 3. Organic carbon content at selected sediment depths (% dry weight) before and after the flood. Uncertainty in OC is ± 0.3 %.

Depth interval	Pre-flood OC	Post-flood OC
(cm)	(% dw)	(% dw)
0–1	1.8	1.9
4–5	1.5	2.0
9–10	1.5	1.3
20–25	0.9	1.5
25–30	1.0	1.6

OC content of 1.7 ± 0.3 %; for this same period the model simulated an average OC of 1.8 % dw. Like the ^{7}Be profile, two possibly distinct regions were delineated in the OC content profile. In the upper 10 cm of sediment, organic carbon content varied from 2 % to 1.3 % after the flood deposition. Below, a slight increase in OC concentration was observed with a subsurface maximum of 1.6 %. In the bottom layer, the average OC concentration was larger after the flood (1.5 ± 0.3 %) than before the flood (0.95 ± 0.3 %) and was similar to the average OC concentration in the top layer before the flood (1.6 ± 0.3 % dw). As the vertical resolution of the measurement of OC content is coarse in comparison to the beryllium profile, we did not attempt to correlate these two profiles.

4 Discussion

Extreme events, such as floods and storms, have measurable impacts on coastal benthic ecosystems near large river mouths and deltas (Tesi et al., 2012; Pastor et al., 2018). The present study provides a temporal picture of the impact of large sediment deposition on sediment biogeochemistry during the winter flooding event of 2021/22 at a shallow station in the Rhône River prodelta. Using a combined data–model approach, we describe prominent features of this flood and their implications for carbon cycling in sediments, the evolution of diagenetic pathways and sulfate/methane transformation during early diagenesis.

4.1 Disturbance identification, flooding and its deposit

The massive deposition of fresh sediments deeply modifies the quantity and quality of the OM and defines the so-called flood layer. Accurate identification of the flood signature and its thickness, deposition timing and composition, which is essential for proper model calibration, is challenging. In most instances, the exact specification of when and where the sediment delivered via a flood event is permanently deposited on the seafloor is highly uncertain (Tesi et al., 2012) due to possible physical mixing with the layer underneath or biomixing (Wheatcroft, 1990). Furthermore, while the thickness of the deposited materials during this type of event is an important marker that can be clearly distinguished, it can be smudged by other related events such as fluctuating deposition–erosion events (Bentley and Nittrouer, 2003; Wheatcroft et al., 2006). For large gauged rivers, the water discharge that characterizes floods is generally well documented (Zebracki et al., 2015). However, the solid discharge is generally less understood due to challenges in accurately sampling sediment during the flood periods.

The average Rhône River water flow was 1470 $m^3 s^{-1}$ in the winter season of 2021/22, with short periods of significantly higher discharge. There were four periods of increased flow, but only one exceeded the flood threshold of 3000 $m^3 s^{-1}$ at the end of December. This main winter flood corresponds well with the high concentrations of suspended particulate materials observed in the Rhône River (Fig. 2). Furthermore, Pont et al. (2002) highlighted the non-linear relationship between flows and SPM concentrations, which corresponds to a large particle discharge at the end of December. Accordingly, a period of time with a single large flood (that is simulated in the model) in the Rhône River prodelta station characterizes this study. This assumption is furthermore supported by the work of Miralles et al. (2005).

In the absence of visual determination of the deposited flood layer, such as variations in the sediment color and texture, we investigated other indicators to evaluate the thickness of the flood layer. The downward shift of the dissolved sulfate gradient (SO_4^{2-}) as well as the gradient of DIC/CH_4 recorded 15 d after the flood was used to determine the extent

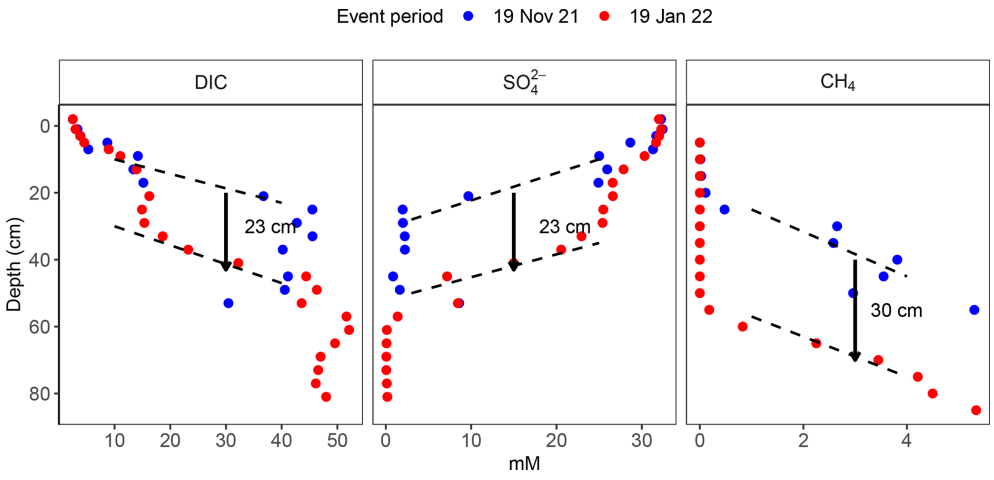

Figure 5. Concentration profiles of DIC, SO_4^{2-} and CH_4 in sediments porewaters from station Z. The dashed lines correspond to the position of the main gradient before (blue dots) and after (red dots) the flood. The arrow symbolizes the shift of this main gradient following the main winter flood.

of the flood deposition. Our estimate amounts to an average of 25 cm (Fig. 5). In this example, we used the difference between 19 November 2021 and 19 January 2022. Using other pre-flood profiles would provide a similar estimate of the deposition thickness, as pre-flood profiles are very comparable (Fig. 3).

This deposition thickness was validated by analyzing ^{7}Be concentrations measured during this time period, which revealed significant activities in the first 30 cm of the sediment (Fig. 4). This latter method that allows for the identification of recent sediment deposition of riverine origin has been widely used in other studies documenting flood deposition processes over short timescales (Feng et al., 1999; Palinkas et al., 2005; Wu et al., 2018). Indeed, ^{7}Be is significantly detected until 30 cm depth (Fig. 4), which indicates newly deposited particles originating from the river down to this particular depth. However, the event layer thicknesses using ^{7}Be can be overestimated in locations where bioturbation activity by benthic fauna is non-negligible. In the Rhône River prodelta, this is not the case as previous studies have shown that the bioturbation rate is low at this location (Pastor et al., 2011b; Pruski et al., 2015) and probably even lower during flood deposition due to habitat disturbance. In general, combining the qualitative assessment of the shift in the post-flood profile relative to the pre-flood, as well as ^{7}Be event-based data, helps in defining our estimate for the deposit thickness. The accurate establishment of this thickness deposit by the flood provides an important constraint to the numerical model and increases its overall skillfullness.

The organic carbon concentration (Table 3) also changes at depth due to the flood deposit. The low concentration of organic carbon observed below 25 cm before the flood is replaced by larger OC concentration after the deposit. Furthermore, the new OC concentrations at depth are similar to those found in the top layer before the flood. This clearly indicates a downward shift of the former interface to a depth of 20–25 cm.

4.2 Transient evolution of mineralization pathways and rates

The accumulation of large quantities of terrigenous materials in the proximal region of the deltaic depocenter has large implications for the carbon cycle (Hedges and Keil, 1995). This routing of carbon to the depocenter sediments results in substantial organic matter degradation despite acting as an accumulation site (Jahnke et al., 1990; Cathalot et al., 2010; Cai 2011; Blair and Aller, 2012). The transformation and short-term fate of riverine OC under the influence of episodic events, however, are largely unknown (Carlin et al., 2021). In the Rhône River prodelta, the model estimate of total organic carbon mineralization was around 148 mmol C m^{-2} d^{-1} before the flood deposition. This estimate is comparable to the total mineralization rate reported in previous studies in the Rhône River prodelta. Under steady-state conditions, Pastor et al. (2011a) reported a total mineralization rate of 150 mmol C m^{-2} d^{-1}, while the integrated mineralization rate in Ait Ballagh et al. (2021) averaged around 145 mmol C m^{-2} d^{-1} for the proximal zone of the prodelta. As reported for other coastal systems with organic-rich sediments, anoxic diagenetic pathways involving organoclastic sulfate reduction (OSR) dominated in terms of the contribution to total OC mineralization.

Prior to the flood event, strong sulfate consumption in the surficial sediment was observed in the measured data, as evidenced by a significant decrease in concentration between 10 and 40 cm, accompanied by a significant increase in DIC concentration. DIC accumulation in intermediate sediment layers was also very large for this time period. This pre-flood situation hints at a system under steady-state conditions. The

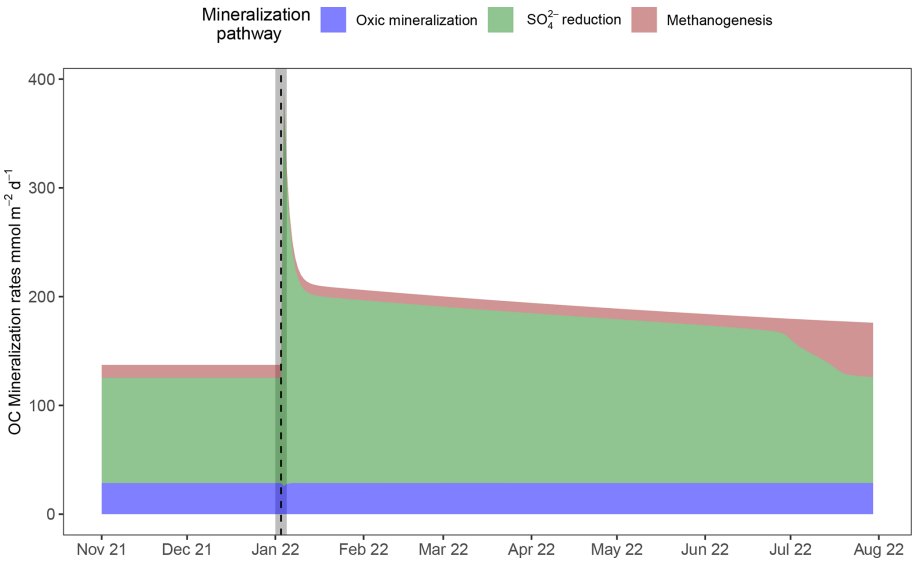

Figure 6. Vertically integrated rate of organic carbon mineralization in the sediment of station Z and relative contributions by different pathways. The grey bar and dashed line indicate the date of the main flood (6 January 2022).

combined contribution of sulfate reduction and methanogenesis (> 70 % of the total mineralization rate) corresponds to values observed in other studies in this shallow region of the prodelta where the anoxic contribution to OC mineralization ranged from 75 % to 89 % (Pastor et al., 2011a, and references therein; Ait Ballagh et al., 2021).

After the flood, the deposition of a thick sediment layer drastically altered the vertical distribution of all profiles with a deeper sulfate penetration, a lower DIC concentration in the top 25 cm of sediment porewaters and a deeper depth of CH_4 appearance. As a result, model calculations suggest an immediate burst followed by an increase in sulfate reduction rates by 75 % (Fig. 6) in comparison to the pre-flood period. As the total rate of OC mineralization increased, the relative contribution of OSR to the total mineralization grew from 65 %, before the flood, to 81 %, after the flood. The relative contribution of methanogenesis to the total OC mineralization rate decreased from 8 % to 4 % after the flood. At the same time, oxic mineralization, which accounts for around 19 % of total mineralization before the flood, was not modified after the flood due to its very short (daily) relaxation time (Nmor et al., 2022), and its share in total mineralization decreases to 11 %. Thus, immediately after the flood and in the following 2 months, OSR was largely favored among the diagenetic pathways in the sediments. This can be related to the large quantity of sulfate available after the flood deposition, which traps sulfate-rich bottom water over the 25 cm added to the sedimentary column, and to its thermodynamically favorable energy yield compared to methanogenesis. These differences in carbon oxidation pathways before and after the flood also reflect the amount and quality of organic matter deposited in the sediment due to the flood input (Marvin-DiPasquale and Capone, 1998; Nmor et al., 2022; Smeaton and Austin, 2022). Indeed, these winter floods carry large amounts of metabolizable organic matter originating from terrestrial organic debris or riverine organic matter (Cathalot et al., 2010; Bourgeois et al., 2011; Pozzato et al., 2018), which may trigger intense recycling once deposited in the sediment (Pastor et al., 2018). In a second time period, unfortunately not covered by the dataset, model simulations indicate that methane contribution increases following complete sulfate relaxation to its pre-flood levels 7 months later. The rate of CH_4 production by methanogenesis increases, reaching 50 mmol C m^{-2} d^{-1}, i.e., 27 % of total mineralization at around 8 months after the event. This secondary increase in methanogenesis needs to be confirmed with new data; it could maintain the long-term relaxation of the system over more than a year for methane, therefore contributing to the accumulation of methane in prodelta sediments (Garcia-Garcia et al., 2006; Nmor, 2023)

4.3 Sulfate–methane dynamics before and after the flood

In anoxic sediments, the carbon cycle is tightly coupled to sulfur–methane cycles (Jørgensen and Kasten, 2006). The present dataset and model can be used to understand the impact of flood deposition on these coupled cycles. In the case of the sulfur cycle, 90 % of oceanic sulfate reduction takes place in sediments of the continental shelves (Jørgensen, 1982; Jørgensen et al., 2019). The two main pathways for sulfate reduction are organoclastic sulfate reduction (OSR), which depends on the lability and amount of degradable organic matter, and anaerobic oxidation of methane (AOM), where methane is anaerobically oxidized to bicarbonate using SO_4^{2-} as an electron acceptor by a consortium of mi-

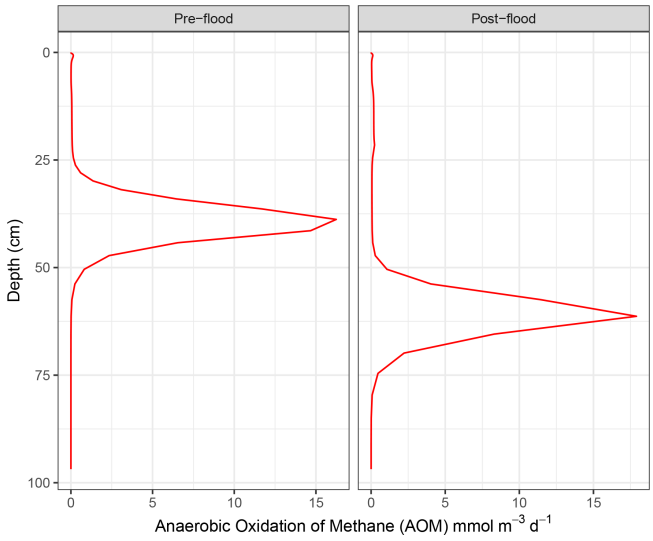

Figure 7. Vertical distribution of anaerobic oxidation of methane (AOM) for the pre-flood and post-flood period.

crobes including bacteria and archaea (Boetius et al., 2000). Although AOM and OSR can coexist, AOM frequently produces a deep sulfate reduction peak that is different from the shallower maximum of sulfate reduction by carbon oxidation, as it essentially occurs in the SMTZ with low SO_4^{2-} concentrations (Regnier et al., 2011). The relative degree of sulfate reduction in both modes regulates the flux of SO_4^{2-} and CH_4 across the SWI (Egger et al., 2018).

The sedimentary CH_4 flux is largely controlled by the rate of AOM; for this reason it is critical to understand how CH_4 and SO_4^{2-} fluxes are regulated (Dale et al., 2006), especially during flood times and following evolution which disrupts the steady-state control of the CH_4 flux. In sediments of the Rhône River prodelta, while bacterial-mediated sulfate reduction is the main oxidation process of OC, the quantification of the contribution of anaerobic oxidation of methane is missing from previous studies (Pastor et al., 2011a; Zhuang et al., 2018; Ait Ballagh et al., 2021). In this study, the data–model approach allows us to quantify the magnitude of the rate of AOM in the sediment.

The depth of maximum AOM before the winter deposition was situated at 35 cm (Fig. 7). The rate of AOM at this depth was 16 mmol m^{-3} d^{-1}. This is higher than values reported in marine sediments from the Skagerrak (5 mmol m^{-3} d^{-1}; Knab et al., 2008) and the Baltic Sea (14 mmol m^{-3} d^{-1}; Treude et al., 2005) but significantly lower than AOM activities in the Gulf of Mexico or the hydrate ridge off the coast of Oregon (500 mmol m^{-3} d^{-1}; Treude et al., 2003).

After the deposition of the flood layer, the AOM maximum rate remains the same in intensity but is shifted downward in the sediment by 22 cm (Fig. 7). Further cross-examination of the sulfate and methane concentration profiles reveals a physical imprint of the flood deposit on the porewater chemical composition. Our data also show that the penetration depth of SO_4^{2-} and appearance of methane exhibited a shift downward relative to the pre-flood situation, confirming the AOM rate calculation by the model. This generated a downward shift of the sulfate–methane transition zone (SMTZ), defined as the area where sulfate and CH_4 are consumed simultaneously. This SMTZ depth below the seafloor acts as a proxy for CH_4 fluxes (Borowski et al., 1999). In general, the presence or absence of externally compressed upward fluid flow (Regnier et al., 2011), the occurrence of localized pockmarks where advective transport occurs (Knab et al., 2008), and organic matter load all influence the depth of the SMTZ. In our case, the observation of the porewater profiles and the SMTZ suggests a deepening with depth following the introduction of the 25 cm flood layer. Prior to the flood deposition, the SMTZ estimated by the data was located between 30 and 40 cm, whereas the model estimated the precise location of the SMTZ at 38 cm. This SMTZ depth shifted to 60 cm after the flood deposition. This vertical shift of the SMTZ in RiOMar systems, like the Rhône prodelta, differs from other coastal areas where a shoaling of the SMTZ is experienced as a result of high loads of organic matter driven by eutrophication (Crill and Martens, 1983). In our case, the deep penetration of bottom-water sulfate following the event indicates that the CH_4-generating processes occur much deeper. Furthermore, the upward diffusion of the released CH_4 (Borowski et al., 1999) is rather slow. This sluggish flux of CH_4 to the SMTZ due to slow molecular diffusion of CH_4 (Regnier et al., 2011) is linked to the long relaxation timescale associated with processes occurring deep in the sediment (Nmor et al., 2022). Our data provide support for this hypothesis and show that the SMTZ in the pre-flood profiles did not change. It is noteworthy that in some other rapid-accumulation settings, increased organic matter loads can change the depth of the SMTZ by bringing it closer to the sediment surface (Crill and Martens, 1983; Dale et al., 2019; Myllykangas et al., 2020). The dynamics of this change are unknown and depend on SO_4^{2-} exhaustion by early diagenesis processes. If this is the case, our observation here offers a different view of the role of instantaneous massive flooding in sulfur–methane dynamics. This may be due to the low "reactivity" of the organic matter or the short timescale associated with the present study, but further investigation of this topic needs to be done to understand the impact of large-deposition events.

Quantitative assessment of the data-based DIC : SO_4^{2-} ratio ($r_{c:s}$) in the sediment cores between pre- and post-flood profiles reveals a drastic change in the stoichiometric ratios involving sulfate reduction partitioned by depth in the new sediment layer (Fig. 8). Before the winter flood, the $r_{c:s}$ varies between -1.7 and -1.4, with no clear pattern distinguishing the upper and lower zones of the sediment favored by either OSR or AOM. The sudden occurrence of the large sediment deposition triggers a post-flood bifurcation in sulfate reduction delineated by the SMTZ. In the newly de-

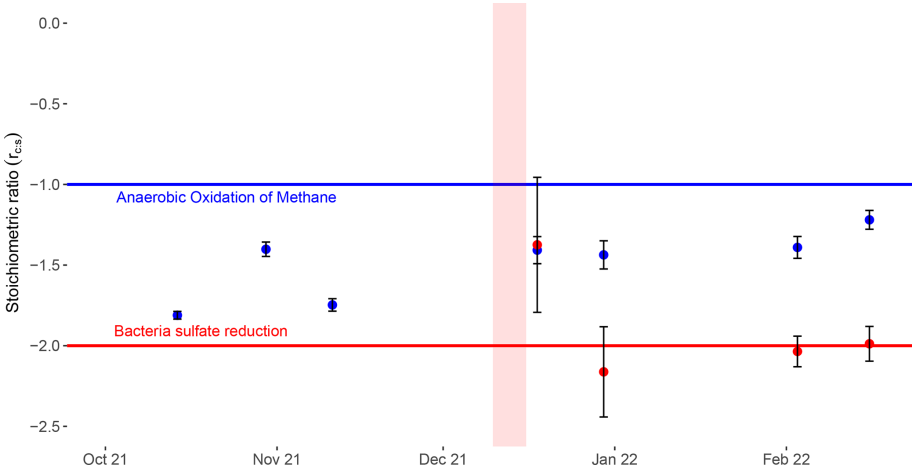

Figure 8. Temporal variation in DIC : SO_4^{2-} porewater ratio ($r_{c:s}$) calculated at the surface or at the depth of the sediment layer. The red bar indicates the flood period; before the flood the entire core is considered to be like the surface layer. Red dots represent the surface sediment layer (flood layer < 25 cm), and blue dots represent the bottom sediment layer (former sediment). The blue line indicates the theoretical stoichiometric ratio of the anaerobic oxidation of methane (-1), and the red line indicates the theoretical stoichiometric ratio of the sulfate reduction (-2).

posited layer, $r_{c:s}$ decreases from -1.8 to -2.0, thus showing a strong tendency toward OSR with time, whereas deeper sediment shows dominant AOM, with $r_{c:s}$ slowly drifting to -1.1 in February (Fig. 8).

The implications of this event-driven drift between the upper and lower sediment are still unclear. However, the link between the temporal movement of the CH_4 front and the migration of the AOM activity to changing conditions has previously been highlighted (Regnier et al., 2011). While the model used here does not explicitly resolve the biomass involved in the reactions (Dale et al., 2008) or consider the impact of bioenergetics (Dale et al., 2006), we show that a shift in the SMTZ is correlated with the depth of maximum AOM rate before and after the deposition (Fig. 7). Since SO_4^{2-} and CH_4 data are correctly reproduced by the model, the depth of the maximum AOM rate is thus essentially controlled by methane availability. This deepening of the AOM maximum suggests that in the advent of flood deposition, the AOM traps the upward flux of methane more efficiently. It has been suggested that the advent of a shallower SMTZ would provide a larger chance of methane escaping from the sediment to the overlying water and, ultimately, to the atmosphere (Borges and Abril, 2011). Thus, the occurrence of this large deposition and the associated downward shift of the SMTZ could increase the efficiency of CH_4 trapping in sediments.

4.4 Flood-induced fluxes and link to carbonate chemistry

Coastal sediment represents an important source of CO_2 to the coastal ocean and to the atmosphere (Egger et al., 2016). Changes in the intensity of various mineralization processes

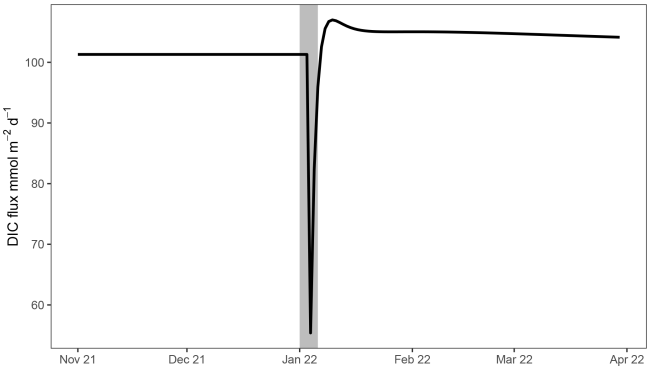

Figure 9. Flux of DIC across the sediment–water interface. Positive flux is directed from the sediment to the overlying bottom water. The grey bar indicates the date of the main flood (6 January 2022).

in response to flood deposition raise concerns about the consequences for fluxes of dissolved inorganic carbon at the sediment–water interface. These fluxes may have a broader impact on benthic–pelagic biogeochemistry, such as ocean acidification (CO_2) of the coastal waters. Current estimates of solute release do not explicitly account for these event-driven sedimentation occurrences, which might have different geochemical properties depending on the type of flood (Cathalot et al., 2010; Pruski et al., 2015). For example, our results show that the event deposits have higher percent OC values and drive larger mineralization rates (Fig. 6), which result in substantial changes in the sediment interstitial composition and possibly fluxes.

A remarkable change in the benthic exchange across the sediment–water interface was observed for DIC (Fig. 9). Before the flood deposition, the DIC flux out of the sediment

amounted to 101 mmol m^{-2} d^{-1}. This calculated DIC efflux is larger than previous data-based estimates but remains on the same order of magnitude as flux estimates reported in this proximal zone (18–78 mmol m^{-2} d^{-1}; Rassmann et al., 2020) as well as other river deltas: Mississippi River delta sediment (36–53 mmol m^{-2} d^{-1}; Rowe et al., 2002), the Fly River delta (35–42 mmol m^{-2} d^{-1}; Aller et al., 2008) and the Guadalquivir River estuary (36–46 mmol m^{-2} d^{-1}; Ferrón et al., 2009). After the flood deposition, the model estimates of DIC benthic flux decreased from 101 to 55 mmol m^{-2} d^{-1} in response to the new input. This was largely related to the large decrease in the DIC gradient in porewaters after the flood (Fig. 3) and represents a 45 % reduction in DIC flux out of the sediment shortly after flood deposition. The reduced DIC flux rapidly reverted to the previous situation after a week of lower fluxes and stabilized to a value of a few percent above the initial value. Yet, the production of DIC in the sediment column had increased by 43 % due to the sudden increase in OC recycling activity following the introduction of fresh organic carbon contained in the flood deposit (Fig. 9). The initial decrease in the flux of DIC was followed by a slight increase of about 4 % and then a stabilization at almost the same initial value as before the flood, indicating that most of the DIC produced by the flood deposit is stored in the sediment porewaters. This is obvious from the DIC profile, which clearly indicates an accumulation of DIC in porewaters after the flood along the measurement period (from January to March).

This change in DIC flux in response to the abrupt introduction of flood-driven deposit can have an impact on the contribution of coastal sediments to the release of CO_2 to the coastal zone and potentially later to the atmosphere. The extent of this gas exchange is determined by several factors, including the DIC / total alkalinity (TA) flux ratio (Andersson and Mackenzie, 2012). In the Rhône prodelta sediments, the total alkalinity flux ranges from 14 to 74 mmol m^{-2} d^{-1}, thus acting as an efficient counteracting mechanism controlling DIC fluxes to the overlying water (Rassmann et al., 2020). As most of the increase in DIC production came from organoclastic sulfate reduction, which has a DIC / TA production ratio of 1 (Rassmann et al., 2020), the flux of alkalinity out of the sediment would probably follow the DIC flux, therefore bringing few changes to the DIC / TA ratio in the coastal bottom waters (Hu and Cai, 2011). However, other contributors to sediment alkalinity such as calcium carbonate dissolution as well as potential coupling processes involving FeS and FeS_2 burial might well affect the alkalinity during relaxation of the system after the flood (Nmor, 2023). This is likely the case in the Rhône River prodelta sediment, where substantial pyrite burial at depth has been reported (Rassmann et al., 2020). As direct measurements of DIC and total alkalinity fluxes during this winter flood are unavailable and porewater iron and sulfide were not monitored during the time series, we can only speculate with the model results. In any case, the magnitude of the DIC flux decrease and its internal storage in surface sediment porewaters highlight the need to better study this phenomenon and provide better constraints on its contribution to the coastal carbon cycle.

5 Conclusion

Extreme flood deposition events produce transient dynamics in biogeochemical processes in coastal marine environments. In this paper, we documented the temporal features of the porewater short-term response over 2 months to organic matter flood input at a station located in the Rhône prodelta. Using a data–model approach, we showed that the introduction of this new layer of OM input from flood deposition can alter the porewater profiles of SO_4^{2-}, DIC and CH_4. Although the model incorporates some simplifying assumptions, FESDIA is able to reproduce accurately the measured concentration depth profiles, including time and space variations. This reflects the capability of the model to capture non-steady-state dynamics driven by abruptly changing boundary conditions.

Our modeling results indicate that large amounts of sediment can also trigger intense biogeochemical processes with the stimulation of sulfate reduction and immediate decline in DIC flux out of the sediment. The internal storage of DIC in porewaters indicates a relative decoupling of sediment organic matter mineralization and fluxes to the water column. By considering the measured porewater profiles and the reactions' stoichiometry, we showed that massive deposition of sediment can result in a disconnection between anaerobic oxidation of methane and the organoclastic pathway for sulfate reduction in the sediment. This decoupling of AOM and OSR implies an increase in the efficiency of the sediment capacity to trap the upward flux of methane. The immediate consequence of the changes in the porewater chemistry and processes following these events highlights their importance to the short- to medium-term response and system functioning in the respective biogeochemical cycle. On a longer timescale, the complete relaxation time that is potentially longer than the return time of disturbing events may also influence benthic biogeochemical fluxes. It is urgently needed to address the issue of multi-seasonal evolution of the sedimentary system after flood deposition together with the potential interaction between successive flood deposits. Clearly, the long-term impact of such events on sediment biogeochemical processes will require better and more continuous field monitoring to help future model development that addresses the biogeochemical consequences of these flood events.

Code and data availability. All data used in this study are available through SEANOE (https://doi.org/10.17882/96514) (Ferreira et al., 2023). The model version used to produce the results in this paper is archived on Zenodo (https://doi.org/10.5281/zenodo.6369288) (Nmor et al., 2022).

Author contributions. EF, SN, EV, BB, BL, CG and CR conceptualized the study. EF, SN, BB, ER, GM, PvB and CR contributed to the data curation. EF, SN, CG and PvB performed the formal analysis. CR acquired the funds. EF, SN, EV, BB, BL, ER, CG, PvB and CR undertook the investigation. EF, SN, EV, BB, BL and CR contributed to the methodology. BB, CG and CR were behind the project administration and the supervision of the research planning. SN, EV and CR contributed to the software development. EF and SN contributed equally to the visualization and the writing of the original draft preparation. All authors contributed to the writing review, editing and validation.

Competing interests. The contact author has declared that none of the authors has any competing interests.

Disclaimer. Publisher's note: Copernicus Publications remains neutral with regard to jurisdictional claims made in the text, published maps, institutional affiliations, or any other geographical representation in this paper. While Copernicus Publications makes every effort to include appropriate place names, the final responsibility lies with the authors.

Acknowledgements. The authors would like to acknowledge Nolwenn Verpy, Laure Papillon and Deny Malengros for help collecting samples; Caroline Gauthier for help with OC analysis; and Marc Souhaut and Thomas Zambardi for help with 7-beryllium analysis at the LAFARA underground laboratory. We would like to thank Hugo Lepage for discussing river flows and helping us obtain the SPM data and also the Observatoire des Sédiments du Rhône staff for the SPM results. Finally, we would also like to thank the various members of the RV *Antédon II* crew who were present on several campaigns. The map in this study was created with the Ocean Data View (ODV) software (Schlitzer, Reiner, Ocean Data View, https://odv.awi.de, last access: 7 September 2023). We thank the associate editor Jack Middelburg and the editorial support team at Copernicus Publications for their assistance during the submission process. We thank Anniet Laverman and the anonymous reviewer for comments and suggestions which improved the quality of the manuscript.

Financial support. This work was supported by a grant from the special call on estuaries from the French national programme EC2CO under the name "DeltaRhone" and a French government grant managed by the Agence Nationale de la Recherche under the France 2030 program, RiOMar reference ANR 22 POCE 0006.

Review statement. This paper was edited by Jack Middelburg and reviewed by Anniet Laverman and one anonymous referee.

References

Aguilera, D. R., Jourabchi, P., Spiteri, C., and Regnier, P.: A knowledge-based reactive transport approach for the simulation of biogeochemical dynamics in Earth systems, Geochem. Geophy. Geosy., 6, 1525–2027, https://doi.org/10.1029/2004GC000899, 2005.

Ait Ballagh, F. E., Rabouille, C., Andrieux-Loyer, F., Soetaert, K., Lansard, B., Bombled, B., Monvoisin, G., Elkalay, K., and Khalil, K.: Spatial Variability of Organic Matter and Phosphorus Cycling in Rhône River Prodelta Sediments (NW Mediterranean Sea, France): a Model-Data Approach, Estuar. Coast., 44, 1765–1789, https://doi.org/10.1007/s12237-020-00889-9, 2021.

Aller, R. C.: Mobile deltaic and continental shelf muds as suboxic, fluidized bed reactors, Mar. Chem., 61, 143–155, https://doi.org/10.1016/S0304-4203(98)00024-3, 1998.

Aller, R. C., Blair, N. E., Xia, Q., and Rude, P. D.: Remineralization rates, recycling, and storage of carbon in Amazon shelf sediments, Cont. Shelf Res., 16, 753–786, https://doi.org/10.1016/0278-4343(95)00046-1, 1996.

Aller, R. C., Blair, N. E., and Brunskill, G. J.: Early diagenetic cycling, incineration, and burial of sedimentary organic carbon in the central Gulf of Papua (Papua New Guinea), J. Geophys. Res.-Earth, 113, 148–227, https://doi.org/10.1029/2006JF000689, 2008.

Andersson, A. J. and Mackenzie, F. T.: Revisiting four scientific debates in ocean acidification research, Biogeosciences, 9, 893–905, https://doi.org/10.5194/bg-9-893-2012, 2012.

Antonelli, C., Frédérique, E., Rolland, B., Provansal, M., and Sabatier, F.: Suspended sediment and ^{137}Cs fluxes during the exceptional December 2003 flood in the Rhone River, southeast France, Geomorphology, 95, 350–360, https://doi.org/10.1016/j.geomorph.2007.06.007, 2008.

Bauer, J. E., Cai, W.-J., Raymond, P. A., Bianchi, T. S., Hopkinson, C. S., and Regnier, P. A. G.: The changing carbon cycle of the coastal ocean, Nature, 504, 61–70, https://doi.org/10.1038/nature12857, 2013.

Bentley, S. J. and Nittrouer, C. A.: Emplacement, modification, and preservation of event strata on a flood-dominated continental shelf: Eel shelf, Northern California, Cont. Shelf Res., 23, 1465–1493, https://doi.org/10.1016/j.csr.2003.08.005, 2003.

Berg, P.: Dynamic Modeling of Early Diagenesis and Nutrient Cycling. A Case Study in an Artic Marine Sediment, Am. J. Sci., 303, 905–955, https://doi.org/10.2475/ajs.303.10.905, 2003.

Berner, R. A.: Early Diagenesis: A Theoretical Approach, Princeton University Press, Princeton, 241 pp., ISBN 9780691082608, 1980.

Bianchi, T. S., Cui, X., Blair, N. E., Burdige, D. J., Eglinton, T. I., and Galy, V.: Centers of organic carbon burial and oxidation at the land-ocean interface, Org. Geochem., 115, 138–155, https://doi.org/10.1016/j.orggeochem.2017.09.008, 2018.

Blair, N. E. and Aller, R. C.: The Fate of Terrestrial Organic Carbon in the Marine Environment, Annu. Rev. Mar. Sci., 4, 401–423, https://doi.org/10.1146/annurev-marine-120709-142717, 2012.

Boetius, A., Ravenschlag, K., Schubert, C. J., Rickert, D., Widdel, F., Gieseke, A., Amann, R., Jørgensen, B. B., Witte, U., and Pfannkuche, O.: A marine microbial consortium apparently mediating anaerobic oxidation of methane, Nature, 407, 623–626, https://doi.org/10.1038/35036572, 2000.

Borges, A. V. and Abril, G.: 5.04 – Carbon Dioxide and Methane Dynamics in Estuaries, in: Treatise on Estuarine and Coastal Science, edited by: Wolanski, E. and McLusky, D., Academic Press, Waltham, https://doi.org/10.1016/B978-0-12-374711-2.00504-0, 119–161, 2011.

Borowski, W. S., Paull, C. K., and Ussler, W.: Global and local variations of interstitial sulfate gradients in deep-water, continental margin sediments: Sensitivity to underlying methane and gas hydrates, Mar. Geol., 159, 131–154, https://doi.org/10.1016/S0025-3227(99)00004-3, 1999.

Bourgeois, S., Pruski, A. M., Sun, M.-Y., Buscail, R., Lantoine, F., Kerhervé, P., Vétion, G., Rivière, B., and Charles, F.: Distribution and lability of land-derived organic matter in the surface sediments of the Rhône prodelta and the adjacent shelf (Mediterranean Sea, France): a multi proxy study, Biogeosciences, 8, 3107–3125, https://doi.org/10.5194/bg-8-3107-2011, 2011.

Bourrin, F., Friend, P. L., Amos, C. L., Manca, E., Ulses, C., Palanques, A., Durrieu de Madron, X., and Thompson, C. E. L.: Sediment dispersal from a typical Mediterranean flood: The Têt River, Gulf of Lions, Cont. Shelf Res., 28, 1895–1910, https://doi.org/10.1016/j.csr.2008.06.005, 2008.

Burdige, D. J.: Burial of terrestrial organic matter in marine sediments: A re-assessment, Global Biogeochem. Cy., 19, 886–6236, https://doi.org/10.1029/2004GB002368, 2005.

Burdige, D. J. and Komada, T.: Anaerobic oxidation of methane and the stoichiometry of remineralization processes in continental margin sediments, Limnol. Oceanogr., 56, 1781–1796, https://doi.org/10.4319/lo.2011.56.5.1781, 2011.

Cai, W.-J.: Estuarine and Coastal Ocean Carbon Paradox: CO2 Sinks or Sites of Terrestrial Carbon Incineration?, Annu. Rev. Mar. Sci., 3, 123–145, https://doi.org/10.1146/annurev-marine-120709-142723, 2011.

Canfield, D. E.: The evolution of the Earth surface sulfur reservoir, Am. J. Sci., 304, 839–861, https://doi.org/10.2475/ajs.304.10.839, 2004.

Canfield, D. E. and Thamdrup, B.: Towards a consistent classification scheme for geochemical environments, or, why we wish the term 'suboxic' would go away, Geobiology, 7, 385–392, https://doi.org/10.1111/j.1472-4669.2009.00214.x, 2009.

Carlin, J. A., Schreiner, K. M., Dellapenna, T. M., McGuffin, A., and Smith, R. W.: Evidence of recent flood deposits within a distal shelf depocenter and implications for terrestrial carbon preservation in non-deltaic shelf settings, Mar. Geol., 431, 106376, https://doi.org/10.1016/j.margeo.2020.106376, 2021.

Cathalot, C., Rabouille, C., Pastor, L., Deflandre, B., Viollier, E., Buscail, R., Grémare, A., Treignier, C., and Pruski, A.: Temporal variability of carbon recycling in coastal sediments influenced by rivers: assessing the impact of flood inputs in the Rhône River prodelta, Biogeosciences, 7, 1187–1205, https://doi.org/10.5194/bg-7-1187-2010, 2010.

Charmasson, S., Radakovitch, O., Arnaud, M., Bouisset, P., and Pruchon, A.-S.: Long-core profiles of ^{137}Cs, ^{134}Cs, ^{60}Co and ^{210}Pb in sediment near the Rhône River (Northwestern Mediterranean Sea), Estuaries, 21, 367–378, https://doi.org/10.2307/1352836, 1998.

Crill, P. M. and Martens, C. S.: Spatial and temporal fluctuations of methane production in anoxic coastal marine sediments, Limnol. Oceanogr., 28, 1117–1130, https://doi.org/10.4319/lo.1983.28.6.1117, 1983.

Dai, Z.-j., Mei, X., Darby, S., Yaying, L., and Li, W.: Fluvial sediment transfer in the Changjiang (Yangtze) river-estuary depositional system, J. Hydrol., 566, 22–1694, https://doi.org/10.1016/j.jhydrol.2018.09.019, 2018.

Dale, A. W., Regnier, P., and Cappellen, P. V.: Bioenergetic Controls on Anaerobic Oxidation of Methane (AOM) in Coastal Marine Sediments: A Theoretical Analysis, Am. J. Sci., 306, 246–294, https://doi.org/10.2475/ajs.306.4.246, 2006.

Dale, A. W., Van Cappellen, P., Aguilera, D. R., and Regnier, P.: Methane efflux from marine sediments in passive and active margins: Estimations from bioenergetic reaction–transport simulations, Earth Planet. Sc. Lett., 265, 329–344, https://doi.org/10.1016/j.epsl.2007.09.026, 2008.

Dale, A. W., Flury, S., Fossing, H., Regnier, P., Røy, H., Scholze, C., and Jørgensen, B. B.: Kinetics of organic carbon mineralization and methane formation in marine sediments (Aarhus Bay, Denmark), Geochim. Cosmochim. Ac., 252, 159–178, https://doi.org/10.1016/j.gca.2019.02.033, 2019.

Day, J., Ibáñez, C., Pont, D., and Scarton, F.: Status and Sustainability of Mediterranean Deltas: The Case of the Ebro, Rhône, and Po Deltas and Venice Lagoon, Coasts and Estuaries, 237–249, https://doi.org/10.1016/B978-0-12-814003-1.00014-9, 2019.

De Borger, E., Tiano, J., Braeckman, U., Rijnsdorp, A. D., and Soetaert, K.: Impact of bottom trawling on sediment biogeochemistry: a modelling approach, Biogeosciences, 18, 2539–2557, https://doi.org/10.5194/bg-18-2539-2021, 2021.

Durrieu De Madron, X., Abassi, A., Heussner, S., Monaco, A., Aloisi, J. C., Radakovitch, O., Giresse, P., Buscail, R., and Kerherve, P.: Particulate matter and organic carbon budgets for the Gulf of Lions (NW Mediterranean), Oceanol. Acta, 23, 717–730, https://doi.org/10.1016/S0399-1784(00)00119-5, 2000.

Egger, M., Lenstra, W., Jong, D., Meysman, F. J. R., Sapart, C. J., van der Veen, C., Röckmann, T., Gonzalez, S., and Slomp, C. P.: Rapid Sediment Accumulation Results in High Methane Effluxes from Coastal Sediments, PLOS ONE, 11, e0161609, https://doi.org/10.1371/journal.pone.0161609, 2016.

Egger, M., Riedinger, N., Mogollón, J. M., and Jørgensen, B. B.: Global diffusive fluxes of methane in marine sediments, Nat. Geosci., 11, 421–425, https://doi.org/10.1038/s41561-018-0122-8, 2018.

Eglinton, T. I.: Tempestuous transport, Nat. Geosci., 1, 727–728, https://doi.org/10.1038/ngeo349, 2008.

Estournel, C., Mikolajczak, G., Ulses, C., Bourrin, F., Canals, M., Charmasson, S., Doxaran, D., Duhaut, T., de Madron, X. D., Marsaleix, P., Palanques, A., Puig, P., Radakovitch, O., Sanchez-Vidal, A., and Verney, R.: Sediment dynamics in the Gulf of Lion (NW Mediterranean Sea) during two autumn–winter periods with contrasting meteorological conditions, Prog. Oceanogr., 210, 102942, https://doi.org/10.1016/j.pocean.2022.102942, 2023.

Eyrolle, F., Radakovitch, O., Raimbault, P., Charmasson, S., Antonelli, C., Ferrand, E., Aubert, D., Raccasi, G., Jacquet, S., and Gurriaran, R.: Consequences of hydrological events on the delivery of suspended sediment and associated radionuclides from the Rhône River to the Mediterranean Sea, J. Soil. Sediment., 12, 1479–1495, https://doi.org/10.1007/s11368-012-0575-0, 2012.

Feng, H., Cochran, J. K., and Hirschberg, D. J.: ^{234}Th and ^{7}Be as tracers for transport and sources of particle-associated contaminants in the Hudson River estuary, Sci. Total Environ., 237–

238, 401–418, https://doi.org/10.1016/S0048-9697(99)00153-9, 1999.

Ferreira E., Nmor S., Viollier E., Lansard B., Bombled B., Regnier E., Monvoisin G., Grenz C., Van Beek P., and Rabouille C.: Characterization of the benthic biogeochemical dynamics after flood events in the Rhône River prodelta: the data-set, SEANOE [data set], https://doi.org/10.17882/96514, 2023.

Ferrón, S., Alonso-Pérez, F., Ortega, T., and Forja, J.: Benthic respiration on the northeastern shelf of the Gulf of Cádiz (SW Iberian Peninsula), Mar. Ecol.-Progr. Ser., 392, 69–80, https://doi.org/10.3354/meps08240, 2009.

García-García, A., Orange, D., Lorenson, T., Radakovitch, O., Tesi, T., Miserocchi, S., Berné, S., Friend, P. L., Nittrouer, C., and Normand, A.: Shallow gas off the Rhône prodelta, Gulf of Lions, Mar. Geol., 234, 215–231, https://doi.org/10.1016/j.margeo.2006.09.005, 2006.

Hedges, J. I. and Keil, R. G.: Sedimentary organic matter preservation: an assessment and speculative synthesis, Mar. Chem., 49, 81–115, https://doi.org/10.1016/0304-4203(95)00008-F, 1995.

Hu, X. and Cai, W.-J.: The impact of denitrification on the atmospheric CO2 uptake potential of seawater, Mar. Chem., 127, 192–198, https://doi.org/10.1016/j.marchem.2011.09.008, 2011.

Jahnke, R. A., Reimers, C. E., and Craven, D. B.: Intensification of recycling of organic matter at the sea floor near ocean margins, Nature, 348, 50–54, https://doi.org/10.1038/348050a0, 1990.

Jørgensen, B. B.: Mineralization of organic matter in the sea bed—the role of sulphate reduction, Nature, 296, 643–645, https://doi.org/10.1038/296643a0, 1982.

Jørgensen, B. B. and Kasten, S.: Sulfur Cycling and Methane Oxidation, in: Marine Geochemistry, edited by: Schulz, H. D. and Zabel, M., Springer, Berlin, Heidelberg., https://doi.org/10.1007/3-540-32144-6_8, 271–309, 2006.

Jørgensen, B. B., Findlay, A. J., and Pellerin, A.: The Biogeochemical Sulfur Cycle of Marine Sediments, Front. Microbiol., 10, 1664–302X, https://doi.org/10.3389/fmicb.2019.00849, 2019.

Knab, N. J., Cragg, B. A., Borowski, C., Parkes, R. J., Pancost, R., and Jørgensen, B. B.: Anaerobic oxidation of methane (AOM) in marine sediments from the Skagerrak (Denmark): I. Geochemical and microbiological analyses, Geochim. Cosmochim. Ac., 72, 2868–2879, https://doi.org/10.1016/j.gca.2008.03.016, 2008.

Lansard, B., Rabouille, C., Denis, L., and Grenz, C.: Benthic remineralization at the land–ocean interface: A case study of the Rhône River (NW Mediterranean Sea), Estuar. Coast. Shelf S., 81, 544–554, https://doi.org/10.1016/j.ecss.2008.11.025, 2009.

Lee, T.-Y., Huang, J.-C., Lee, J.-Y., Jien, S.-H., Zehetner, F., and Kao, S.-J.: Magnified Sediment Export of Small Mountainous Rivers in Taiwan: Chain Reactions from Increased Rainfall Intensity under Global Warming, PLOS ONE, 10, e0138283, https://doi.org/10.1371/journal.pone.0138283, 2015.

Lepage, H., Gruat, A., Thollet, F., Le Coz, J., Coquery, M., Masson, M., Dabrin, A., Radakovitch, O., Labille, J., Ambrosi, J.-P., Delanghe, D., and Raimbault, P.: Concentrations and fluxes of suspended particulate matter and associated contaminants in the Rhône River from Lake Geneva to the Mediterranean Sea, Earth Syst. Sci. Data, 14, 2369–2384, https://doi.org/10.5194/essd-14-2369-2022, 2022.

Li, Y.-H. and Gregory, S.: Diffusion of ions in sea water and in deep-sea sediments, Geochim. Cosmochim. Ac., 38, 703–714, https://doi.org/10.1016/0016-7037(74)90145-8, 1974.

Lionello, P., Sannino, G., and Vilibić, I.: Surface wave and sea surface dynamics in the Mediterranean, in: Oceanography of the Mediterranean sea: An Introductory Guide, edited by: Schroeder, K., and Chiggiato, J., Elsevier, https://doi.org/10.1016/B978-0-12-823692-5.00007-8, 161–207, 2023.

Liu, J. T., Kao, S.-J., Huh, C.-A., and Hung, C.-C.: Gravity Flows Associated with Flood Events and Carbon Burial: Taiwan as Instructional Source Area, Annu. Rev. Mar. Sci., 5, 47–68, https://doi.org/10.1146/annurev-marine-121211-172307, 2013.

Maillet, G. M., Vella, C., Berné, S., Friend, P. L., Amos, C. L., Fleury, T. J., and Normand, A.: Morphological changes and sedimentary processes induced by the December 2003 flood event at the present mouth of the Grand Rhône River (southern France), Mar. Geol., 234, 159–177, https://doi.org/10.1016/j.margeo.2006.09.025, 2006.

Magen, C., Lapham, L., Pohlman, J. W., Marshall, K., Bosman, S., Casso, M., Chanton, J. P.: A simple headspace equilibration method for measuring dissolved methane, Limnol. Oceanogr.-Meth., 12, 1541–5856, https://doi.org/10.4319/lom.2014.12.637, 2014.

Manh, N. V., Dung, N. V., Hung, N. N., Merz, B., and Apel, H.: Large-scale suspended sediment transport and sediment deposition in the Mekong Delta, Hydrol. Earth Syst. Sci., 18, 3033–3053, https://doi.org/10.5194/hess-18-3033-2014, 2014.

Many, G., Bourrin, F., Durrieu de Madron, X., Ody, A., Doxaran, D., and Cauchy, P.: Glider and satellite monitoring of the variability of the suspended particle distribution and size in the Rhône ROFI, Prog. Oceanogr., 163, 123–135, https://doi.org/10.1016/j.pocean.2017.05.006, 2018.

Marvin-DiPasquale, M. C. and Capone, D. G.: Benthic sulfate reduction along the Chesapeake Bay central channel, I. Spatial trends and controls, Mar. Ecol. Prog. Ser., 168, 213–228, https://doi.org/10.3354/meps168213, 1998.

McKee, B. A., Aller, R. C., Allison, M. A., Bianchi, T. S., and Kineke, G. C.: Transport and transformation of dissolved and particulate materials on continental margins influenced by major rivers: benthic boundary layer and seabed processes, Cont. Shelf Res., 24, 899–926, https://doi.org/10.1016/j.csr.2004.02.009, 2004.

Miralles, J., Radakovitch, O., and jean-claude, A.: ^{210}Pb sedimentation rates from the Northwestern Mediterranean margin, Mar. Geol., 216, 155–167, https://doi.org/10.1016/j.margeo.2005.02.020, 2005.

Moriarty, J. M., Harris, C. K., Fennel, K., Friedrichs, M. A. M., Xu, K., and Rabouille, C.: The roles of resuspension, diffusion and biogeochemical processes on oxygen dynamics offshore of the Rhône River, France: a numerical modeling study, Biogeosciences, 14, 1919–1946, https://doi.org/10.5194/bg-14-1919-2017, 2017.

Mucci, A., Sundby, B., Gehlen, M., Arakaki, T., Zhong, S., and Silverberg, N.: The fate of carbon in continental shelf sediments of eastern Canada: a case study, Deep-Sea Res. Pt. II, 47, 733–760, https://doi.org/10.1016/S0967-0645(99)00124-1, 2000.

Myllykangas, J.-P., Hietanen, S., and Jilbert, T.: Legacy Effects of Eutrophication on Modern Methane Dynamics in a Boreal Estuary, Estuar. Coast., 43, 189–206, https://doi.org/10.1007/s12237-019-00677-0, 2020.

Nmor, S.: Modélisation numérique des événements lors de la diagenèse précoce dans les écosystèmes côtiers: application aux

dépôts de crue dans le prodelta du Rhône, PhD thesis, Laboratoire des Sciences du climat et de l'envrionnement, University Paris-Saclay, France, 2023.

Nmor S. and Soetaert K.: FESDIA: An early diagenesis model including Iron (Fe), Sulfur (S) and Methane (CH_4) dynamics, Zenodo [code], https://doi.org/10.5281/zenodo.6369288, 2022.

Nmor, S. I., Viollier, E., Pastor, L., Lansard, B., Rabouille, C., and Soetaert, K.: FESDIA (v1.0): exploring temporal variations of sediment biogeochemistry under the influence of flood events using numerical modelling, Geosci. Model Dev., 15, 7325–7351, https://doi.org/10.5194/gmd-15-7325-2022, 2022.

Palinkas, C. M., Nittrouer, C., Wheatcroft, R., and Langone, L.: The use of ^{7}Be to identify event and seasonal sedimentation near the Po River delta, Adriatic Sea, Mar. Geol., 222, 95–112, https://doi.org/10.1016/j.margeo.2005.06.011, 2005.

Pastor, L., Cathalot, C., Deflandre, B., Viollier, E., Soetaert, K., Meysman, F. J. R., Ulses, C., Metzger, E., and Rabouille, C.: Modeling biogeochemical processes in sediments from the Rhône River prodelta area (NW Mediterranean Sea), Biogeosciences, 8, 1351–1366, https://doi.org/10.5194/bg-8-1351-2011, 2011a.

Pastor, L., Deflandre, B., Viollier, E., Cathalot, C., Metzger, E., Rabouille, C., Escoubeyrou, K., Lloret, E., Pruski, A. M., Vétion, G., Desmalades, M., Buscail, R., and Grémare, A.: Influence of the organic matter composition on benthic oxygen demand in the Rhône River prodelta (NW Mediterranean Sea), Cont. Shelf Res., 31, 1008–1019, https://doi.org/10.1016/j.csr.2011.03.007, 2011b.

Pastor, L., Rabouille, C., Metzger, E., Thibault de Chanvalon, A., Viollier, E., and Deflandre, B.: Transient early diagenetic processes in Rhône prodelta sediments revealed in contrasting flood events, Cont. Shelf Res., 166, 65–76, https://doi.org/10.1016/j.csr.2018.07.005, 2018.

Pont, D., Simonnet, J. P., and Walter-Simonnet, A. V.: Medium-term Changes in Suspended Sediment Delivery to the Ocean: Consequences of Catchment Heterogeneity and River Management (Rhône River, France), Estuar. Coast. Shelf S., 54, 1–18, https://doi.org/10.1006/ecss.2001.0829, 2002.

Pozzato, L., Rassmann, J., Lansard, B., Dumoulin, J.-P., Breugel, P., and Rabouille, C.: Origin of remineralized organic matter in sediments from the Rhone River prodelta (NW Mediterranean) traced by $\Delta^{14}C$ and $\delta^{13}C$ signatures of pore water DIC, Prog. Oceanogr., 163, 112–122, https://doi.org/10.1016/j.pocean.2017.05.008, 2018.

Pruski, A. M., Buscail, R., Bourgeois, S., Vétion, G., Coston-Guarini, J., and Rabouille, C.: Biogeochemistry of fatty acids in a river-dominated Mediterranean ecosystem (Rhône River prodelta, Gulf of Lions, France): Origins and diagenesis, Org. Geochem., 83–84, 227–240, https://doi.org/10.1016/j.orggeochem.2015.04.002, 2015.

Rabouille, C. and Gaillard, J.-F.: Towards the EDGE: Early Diagenetic Global Explanation. A model depicting the early diagenesis of organic matter, O_2, NO_3, Mn, and PO_4, Geochim. Cosmochim. Ac., 55, 2511–2525, https://doi.org/10.1016/0016-7037(91)90369-G , 1991.

Rassmann, J., Lansard, B., Pozzato, L., and Rabouille, C.: Carbonate chemistry in sediment porewaters of the Rhône River delta driven by early diagenesis (northwestern Mediterranean), Biogeosciences, 13, 5379–5394, https://doi.org/10.5194/bg-13-5379-2016, 2016.

Rassmann, J., Eitel, E. M., Lansard, B., Cathalot, C., Brandily, C., Taillefert, M., and Rabouille, C.: Benthic alkalinity and dissolved inorganic carbon fluxes in the Rhône River prodelta generated by decoupled aerobic and anaerobic processes, Biogeosciences, 17, 13–33, https://doi.org/10.5194/bg-17-13-2020, 2020.

Regnier, P., Dale, A. W., Arndt, S., LaRowe, D. E., Mogollón, J., and Van Cappellen, P.: Quantitative analysis of anaerobic oxidation of methane (AOM) in marine sediments: A modeling perspective, Earth-Sci. Rev., 106, 105–130, https://doi.org/10.1016/j.earscirev.2011.01.002, 2011.

Rowe, G. T., Kaegi, M. E. C., Morse, J. W., Boland, G. S., and Escobar Briones, E. G.: Sediment community metabolism associated with continental shelf hypoxia, Northern Gulf of Mexico, Estuaries, 25, 1097–1106, https://doi.org/10.1007/BF02692207, 2002.

Seeberg-Elverfeldt, J., Schlüter, M., Feseker, T., and Koelling, M.: Rhizon sampling of pore waters near the sediment/water interface of aquatic systems, Limnol. Oceanogr.-Meth., 3, 361–371, https://doi.org/10.4319/lom.2005.3.361, 2005.

Smeaton, C. and Austin, W.: Quality Not Quantity: Prioritizing the Management of Sedimentary Organic Matter Across Continental Shelf Seas, Geophys. Res. Lett., 49, 94–8276, https://doi.org/10.1029/2021GL097481, 2022.

Soetaert, K., Herman, P. M. J., and Middelburg, J. J.: A model of early diagenetic processes from the shelf to abyssal depths, Geochim. Cosmochim. Ac., 60, 1019–1040, https://doi.org/10.1016/0016-7037(96)00013-0, 1996.

Tesi, T., Langone, L., Goñi, M. A., Wheatcroft, R. A., Miserocchi, S., and Bertotti, L.: Early diagenesis of recently deposited organic matter: A 9-yr time-series study of a flood deposit, Geochim. Cosmochim. Ac., 83, 19–36, https://doi.org/10.1016/j.gca.2011.12.026, 2012.

Thill, A., Moustier, S., Garnier, J. M., Estournel, C., Naudin, J., and Bottero, J.-Y.: Evolution of particle size and concentration in the Rhone river mixing zone: Influence of salt flocculation, Cont. Shelf Res., 21, 2127–2140, https://doi.org/10.1016/S0278-4343(01)00047-4, 2001.

Treude, T., Boetius, A., Knittel, K., Wallmann, K., and Jørgensen, B. B.: Anaerobic oxidation of methane above gas hydrates at Hydrate Ridge, NE Pacific Ocean, Mar. Ecol.-Prog. Ser., 264, 1–14, https://doi.org/10.3354/meps264001, 2003.

Treude, T., Krüger, M., Boetius, A., and Jørgensen, B.: Environmental control on anaerobic oxidation of methane in the gassy sediments of Eckernförde Bay (German Baltic), Limnol. Oceanogr., 50, 1771–1786, https://doi.org/10.4319/lo.2005.50.6.1771, 2005.

Ulses, C., Estournel, C., Durrieu de Madron, X., and Palanques, A.: Suspended sediment transport in the Gulf of Lions (NW Mediterranean): Impact of extreme storms and floods, Cont. Shelf Res., 28, 2048–2070, https://doi.org/10.1016/j.csr.2008.01.015, 2008.

Van Beek, P., Souhaut, M., Lansard, B., Bourquin, M., Reyss, J. L., von Ballmoos, P., and Jean, P.: LAFARA: a new underground laboratory in the French Pyrénées for ultra low-level gamma-ray spectrometry, J. Environ. Radioactiv., 116, 152–158, https://doi.org/10.1016/j.jenvrad.2012.10.002, 2013.

Van Cappellen, P. and Gaillard, J.-F.: Chapter 8. Biogeochemical dynamics in aquatic sediments, in: Reactive Trans-

port in Porous Media, edited by: Peter, C. L., Carl, I. S., and Eric, H. O., DeGruyter, Berlin, Boston, 335–376, https://doi.org/10.1515/9781501509797-011, 2018.

Wang, Y. and Van Cappellen, P.: A multicomponent reactive transport model of early diagenesis: Application to redox cycling in coastal marine sediments, Geochim. Cosmochim. Ac., 60, 2993–3014, https://doi.org/10.1016/0016-7037(96)00140-8, 1996.

Wheatcroft, R. A.: Preservation potential of sedimentary event layers, Geology, 18, 843–845, https://doi.org/10.1130/0091-7613(1990)018%3C0843:PPOSEL%3E2.3.CO;2, 1990.

Wheatcroft, R. and Sommerfield, C. K.: River Sediment Flux and Shelf Sediment Accumulation Rates on the Pacific Northwest Margin, Cont. Shelf Res., 25, 311–332, https://doi.org/10.1016/j.csr.2004.10.001, 2005.

Wheatcroft, R., Stevens, A., Hunt, L., and Milligan, T.: The large-scale distribution and internal geometry of the fall 2000 Po River flood deposit: Evidence from digital X-radiography, Cont. Shelf Res., 26, 499–516, https://doi.org/10.1016/j.csr.2006.01.002, 2006.

Wu, J., Rabouille, C., Charmasson, S., Reyss, J. L., and Cagnat, X.: Constraining the origin of recently deposited particles using natural radionuclides ^{7}Be and ^{234}Th$_{ex}$ in deltaic sediments, Cont. Shelf Res., 165, 106–119, https://doi.org/10.1016/j.csr.2018.06.010, 2018.

Zebracki, M., Eyrolle-Boyer, F., Evrard, O., Claval, D., Mourier, B., Gairoard, S., Cagnat, X., and Antonelli, C.: Tracing the origin of suspended sediment in a large Mediterranean river by combining continuous river monitoring and measurement of artificial and natural radionuclides, Sci. Total Environ., 502, 122–132, https://doi.org/10.1016/j.scitotenv.2014.08.082, 2015.

Zhuang, G.-C., Heuer, V. B., Lazar, C. S., Goldhammer, T., Wendt, J., Samarkin, V. A., Elvert, M., Teske, A. P., Joye, S. B., and Hinrichs, K.-U.: Relative importance of methylotrophic methanogenesis in sediments of the Western Mediterranean Sea, Geochim. Cosmochim. Ac., 224, 171–186, https://doi.org/10.1016/j.gca.2017.12.024, 2018.